JVI Journals.ASM.org

Severe Acute Respiratory Syndrome Coronaviruses with Mutations in the E Protein Are Attenuated and Promising Vaccine Candidates

Jose A. Regla-Nava,[a] Jose L. Nieto-Torres,[a] Jose M. Jimenez-Guardeño,[a] Raul Fernandez-Delgado,[a] Craig Fett,[b] Carlos Castaño-Rodríguez,[a] Stanley Perlman,[b] Luis Enjuanes,[a] Marta L. DeDiego[a]*

Department of Molecular and Cell Biology, Centro Nacional de Biotecnología (CNB-CSIC), Darwin 3, Campus Universidad Autónoma de Madrid, Madrid, Spain[a]; Department of Microbiology, University of Iowa, Iowa City, Iowa, USA[b]

ABSTRACT

Severe acute respiratory syndrome coronavirus (SARS-CoV) causes a respiratory disease with a mortality rate of 10%. A mouse-adapted SARS-CoV (SARS-CoV-MA15) lacking the envelope (E) protein (rSARS-CoV-MA15-ΔE) is attenuated *in vivo*. To identify E protein regions and host responses that contribute to rSARS-CoV-MA15-ΔE attenuation, several mutants (rSARS-CoV-MA15-E*) containing point mutations or deletions in the amino-terminal or the carboxy-terminal regions of the E protein were generated. Amino acid substitutions in the amino terminus, or deletion of regions in the internal carboxy-terminal region of E protein, led to virus attenuation. Attenuated viruses induced minimal lung injury, diminished limited neutrophil influx, and increased $CD4^+$ and $CD8^+$ T cell counts in the lungs of BALB/c mice, compared to mice infected with the wild-type virus. To analyze the host responses leading to rSARS-CoV-MA15-E* attenuation, differences in gene expression elicited by the native and mutant viruses in the lungs of infected mice were determined. Expression levels of a large number of proinflammatory cytokines associated with lung injury were reduced in the lungs of rSARS-CoV-MA15-E*-infected mice, whereas the levels of anti-inflammatory cytokines were increased, both at the mRNA and protein levels. These results suggested that the reduction in lung inflammation together with a more robust antiviral T cell response contributed to rSARS-CoV-MA15-E* attenuation. The attenuated viruses completely protected mice against challenge with the lethal parental virus, indicating that these viruses are promising vaccine candidates.

IMPORTANCE

Human coronaviruses are important zoonotic pathogens. SARS-CoV caused a worldwide epidemic infecting more than 8,000 people with a mortality of around 10%. Therefore, understanding the virulence mechanisms of this pathogen and developing efficacious vaccines are of high importance to prevent epidemics from this and other human coronaviruses. Previously, we demonstrated that a SARS-CoV lacking the E protein was attenuated *in vivo*. Here, we show that small deletions and modifications within the E protein led to virus attenuation, manifested by minimal lung injury, limited neutrophil influx to the lungs, reduced expression of proinflammatory cytokines, increased anti-inflammatory cytokine levels, and enhanced $CD4^+$ and $CD8^+$ T cell counts *in vivo*, suggesting that these phenomena contribute to virus attenuation. The attenuated mutants fully protected mice from challenge with virulent virus. These studies show that mutations in the E protein are not well tolerated and indicate that this protein is an excellent target for vaccine development.

Coronaviruses (CoVs) are responsible for a wide range of important veterinary and human diseases (1). Severe acute respiratory syndrome (SARS) is caused by a coronavirus (SARS-CoV) that emerged in Guangdong Province, China, causing the 2002-2003 epidemic, and infecting more than 8,000 individuals with a 10% mortality rate (1–5). A novel human coronavirus, Middle East respiratory syndrome coronavirus (MERS-CoV), was isolated from the sputum of a man with pneumonia and renal failure in Jeddah, Saudi Arabia, in 2012 (6, 7). As of 21 November 2014, the WHO confirmed 909 MERS cases, in which 36% of patients died (8). CoVs similar to SARS-CoV and MERS-CoV have been found in bats distributed across the world from which new zoonotic transmissions into human population could occur (9–15). Therefore, understanding the virulence mechanisms of these pathogens and developing efficacious vaccines and therapies are of high importance.

SARS-CoV is an enveloped virus with a single-stranded, positive-sense, 29.7-kb RNA genome (16, 17). The 5′ two-thirds of the genome comprise two overlapping open reading frames, ORF 1a and ORF 1b, encoding two polyproteins, pp1a and pp1ab. In addition, SARS-CoV encodes a set of structural proteins present in all CoVs: spike (S), membrane (M), envelope (E), nucleocapsid (N), and accessory proteins 3a, 6, 7a, 7b, 8a, 8b, and 9b (18).

SARS-CoV E protein is a small integral membrane protein of

Received 12 December 2014 **Accepted** 14 January 2015

Accepted manuscript posted online 21 January 2015

Citation Regla-Nava JA, Nieto-Torres JL, Jimenez-Guardeño JM, Fernandez-Delgado R, Fett C, Castaño-Rodríguez C, Perlman S, Enjuanes L, DeDiego ML. 2015. Severe acute respiratory syndrome coronaviruses with mutations in the E protein are attenuated and promising vaccine candidates. J Virol 89:3870–3887. doi:10.1128/JVI.03566-14.

Editor: T. S. Dermody

Address correspondence to Luis Enjuanes, L.Enjuanes@cnb.csic.es.

* Present address: Marta L. DeDiego, David H. Smith Center for Vaccine Biology and Immunology, University of Rochester Medical Center, Rochester, New York, USA.

doi:10.1128/JVI.03566-14

TABLE 1 Primers used for the generation of rSARS-CoV-MA15-E* protein deletion mutants

E* mutant	PCR no.	Primer	Sequence (5′→3′)
Δ2 mutant, 24 nt[a]	1	E-SARS-25871-VS	CGTTGTACATGGCTATTTCACCG
	1	E-SARS-26278-RS	GGTTTTACTAAACTCACGTTAACAATAAGCGCAGTAAGGATGGCTAGTGTG
	2	E-SARS-26223-VS	GCGCTTATTGTTAACGTGAGTTTAGTAAAACC
	2	E-SARS-28160-RS	CTGAGTGAGCTGTGAACC
Δ3 mutant, 21 nt	1	E-SARS-25871-VS	CGTTGTACATGGCTATTTCACCG
	1	E-SARS-26299-RS	CGCGAGTAGACGTAAACCGTTGGTTTATTGCAGCAGTACGCACACAATCG
	2	E-SARS-26274-VS	AAACCAACGGTTTACGTCTACTCGCG
	2	E-SARS-28160-RS	CTGAGTGAGCTGTGAACC
Δ4 mutant, 18 nt	1	E-SARS-25871-VS	CGTTGTACATGGCTATTTCACCG
	1	E-SARS-26298-RS	CGCGAGTAGACGTAAACCACGTTAACAATATTGCAGCAGTACGC
	2	E-SARS-26248-VS	GCGTACTGCTGCAATATTGTTAACGTGGTTTACGTCTACTCGCG
	2	E-SARS-28160-RS	CTGAGTGAGCTGTGAACC
Δ5 mutant, 36 nt	1	E-SARS-25871-VS	CGTTGTACATGGCTATTTCACCG
	1	E-SARS-26332-RS	GGAACTCCTTCAGAAGAGTTCAGTACTAAACTCACGTTAACAATATTGC
	2	E-SARS-26266-VS	GTTTAGTACTGAACTCTTCTGAAGGAGTTCC
	2	E-SARS-28160-RS	CTGAGTGAGCTGTGAACC
Δ6 mutant, 36 nt	1	E-SARS-25871-VS	CGTTGTACATGGCTATTTCACCG
	1	E-SARS-26379-RS	CCAAACAGAATAATAATAATAGTTAGTTCGTTTAATTTTTAACACGCGAGTAGACGTAAACCG
	2	E-SARS-26296-VS	CGCGTGTTAAAAATTAAACGAACTAACTATTATTATTATTCTGTTTGG
	2	E-SARS-28160-RS	CTGAGTGAGCTGTGAACC

[a] nt, nucleotides.

76 amino acids. This protein contains a short hydrophilic amino terminus, a hydrophobic region, and a hydrophilic carboxy terminus (19). The hydrophobic region forms one amphipathic α-helix that oligomerizes and displays ion channel activity (20–22). E protein is present in small amounts within viral particles but is abundantly synthesized in infected cells (23–25), where it localizes mainly in the endoplasmic reticulum Golgi intermediate compartment (ERGIC), participating in virus morphogenesis and budding (25–27). SARS-CoV lacking the E gene (rSARS-CoV-ΔE) was attenuated *in vivo* (28, 29) and protected against challenge with virulent SARS-CoV (30–32). The E protein is a virulence factor, regulating cell stress response and apoptosis and promoting inflammation (33).

SARS-CoV causes a respiratory illness characterized by acute lung injury (ALI), and its most severe pathological form is acute respiratory distress syndrome (ARDS). These pathological conditions are characterized by diffuse alveolar damage (DAD), pulmonary cellular infiltration, hyaline membrane formation, and edema accumulation, leading to hypoxemia and eventually to death (34–37). SARS-CoV infection induces migration to the lungs of immune cells, such as neutrophils and macrophages, which initiate and amplify the inflammatory response (38, 39). Accordingly, the levels of several proinflammatory cytokines, including gamma interferon (IFN-γ), IFN-inducible protein 10 (IP-10)/CXCL10, monocyte chemoattractant protein 1 (MCP-1)/CCL2, and several interleukins (IL-1β, IL-6, IL-8, and IL-12), are elevated in the lungs and peripheral blood of SARS patients (40–49). This exacerbated inflammatory process correlates with lung injury and a poor outcome. T cells are essential to resolve SARS-CoV infections. T cell responses play a crucial role in SARS-CoV clearance and in protection from clinical disease (50–52). Accordingly, one notable finding in human SARS, associated with an adverse outcome, was the rapid development of lymphopenia, with numbers of $CD4^+$ T cells more severely reduced than those of $CD8^+$ T cells during acute disease (38, 53–56).

The SARS-CoV Urbani strain virus causes no significant disease in wild-type (wt) mice (57). Passage through BALB/c mouse lungs resulted in a mouse-adapted virus (MA15 strain) (57), which upon infection reproduced many aspects of the human disease, such as high virus titers, pathological changes in lungs, viremia, neutrophilia, and lethality (57). We previously showed that rSARS-CoV-MA15-ΔE was attenuated in mice and that immunization with rSARS-CoV-MA15-ΔE completely protected young and aged BALB/c mice against challenge with a lethal dose of MA15 (32, 58). Furthermore, we showed that SARS-CoV E

TABLE 2 TaqMan assays used to analyze the expression of cellular genes by quantitative RT-PCR

Protein name	TaqMan assay[a]	Description
TNF	Mm00443258-ml	Tumor necrosis factor
IL-4	Mm00445259_ml	Interleukin 4
IL-5	Mm00439646_ml	Interleukin 5
IL-6	Mm00446190-ml	Interleukin 6
IL-10	Mm00439614_ml	Interleukin 10
IL-12B	Mm00434174_ml	Interleukin 12B
IL-13	Mm00434204_ml	Interleukin 13
CXCL1/NAP-3	Mm04207460-ml	Neutrophil-activating protein 3
CXCL2/MIP-2	Mm00436450-ml	Macrophage inflammatory protein 2
CXCL10/IP-10	Mm00445235-ml	Interferon-inducible protein 10
CCL2/MCP-1	Mm00441242-ml	Monocyte chemotactic protein 1
CCL3/MIP1A	Mm00441259_gl	Macrophage inflammatory protein 1α
CCL4/MIP1B	Mm00443111_ml	Macrophage inflammatory protein 1β
IFN-γ	Mm01168134-ml	Gamma interferon
TGF-β	Mm01178820_ml	Transforming growth factor beta 1
18S	Mm03928990-gl	Ribosomic RNA 18S

[a] Mm, *Mus musculus*.

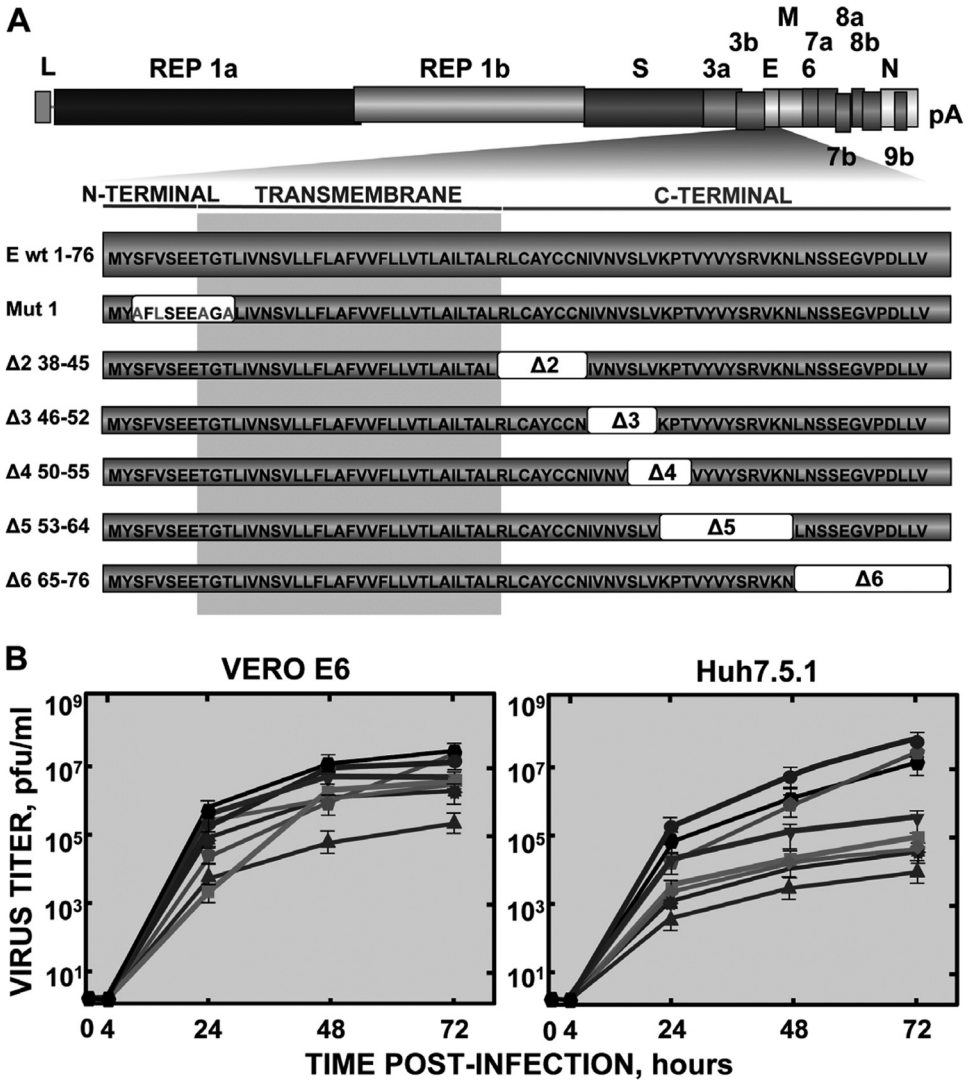

FIG 1 Schematic of mutations and deletions introduced within SARS-CoV E protein and growth kinetics of the mutant viruses (rSARS-CoV-MA15-E*). (A) The SARS-CoV genome is shown in the top, and the expanded region shows the E protein sequence and its different regions. White boxes represent the amino acids deleted within the E protein in each virus. Gray letters indicate the amino acids mutated to change the amino-terminal region of the protein. (B) Mutant virus growth kinetics. Subconfluent monolayers of Vero E6 and Huh7.5.1 cells were infected with wt, ΔE, and rSARS-CoV-MA15-E* viruses at an MOI of 0.001 on Vero E6 cells. Error bars represent standard deviations of the mean using data from three independent experiments. Hexagon, WT; diamond, ΔE; pentagon, Mut 1; triangle, Δ2; star, Δ3; inverted triangle, Δ4; square, Δ5; and circle, Δ6.

protein ion channel activity promoted virus virulence and fitness (37). To identify the E protein regions and the mechanisms leading to SARS-CoV-ΔE attenuation, several mouse-adapted virus mutants encoding amino acid substitutions in the amino terminal or small deletions located in the carboxy-terminal region of the E protein (rSARS-CoV-MA15-E*) were constructed. Amino acid substitutions in the amino terminal, or deletion of regions in the central carboxy-terminal region of E protein, resulted in virus attenuation, accompanied by reductions in lung inflammation, neutrophil influx into the lungs, and proinflammatory cytokine expression. Remarkably, the number of T cells was increased in the lungs of mice infected with the less pathogenic viruses, most probably contributing to their more rapid clearance. Importantly, the attenuated mutants protected against the challenge with the virulent wt virus.

MATERIALS AND METHODS

Cells. Vero E6, BHK, and Huh7.5.1 cells were kindly provided by E. Snijder (University of Leiden, The Netherlands), H. Laude (Unité de Virologie et Immunologie Molecularies, INRA, France), and R. Bartenschlager (Department of Molecular Virology, University of Heidelberg, Germany), respectively, and were propagated as described previously (28).

Viruses. Mouse-adapted SARS-CoV-MA15 (57) was a gift from Kanta Subbarao (National Institutes of Health, Bethesda, MD). Recombinant viruses were rescued from infectious cDNA clones generated in our laboratory (32, 58, 59).

Mice. Specific-pathogen-free BALB/c mice were purchased from the National Cancer Institute at the age of 6 or 16 weeks or from Harlan Laboratories (Holland) at the age of 8 weeks and maintained for 8 additional weeks. All experiments involving SARS-CoV were conducted in biosafety level 3 laboratories in the animal care facility at the University of Iowa or at the Center for Animal Health Research (CISA-INIA, Spain),

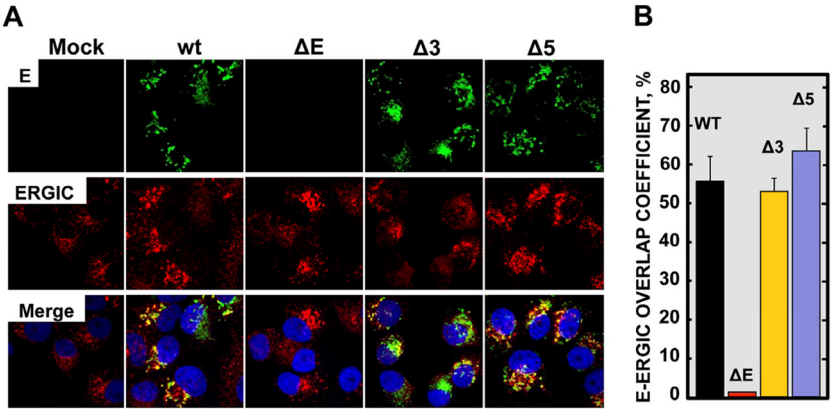

FIG 2 Subcellular localization of mutant E proteins. (A) Vero E6 cells were infected with either rSARS-CoV-MA15-ΔE, -Δ3, or -Δ5 or wt recombinant viruses, at an MOI of 0.3, and fixed at 24 hpi. E protein (green) and ERGIC (red) were labeled with specific antibodies. Nuclei were stained with DAPI (blue). Merge indicates superposition of both labels. Original magnification was ×126. (B) The panel represents the percentage of overlap coefficient between E protein and ERGIC, calculated with Leica LAS AF v2.6.0 software.

equipped with ventilated racks (animal transport unit and biocontainment unit; Allentown, Inc.) to store the animals during the experiment. All the protocols were approved by the EU, by the CISA-INIA Committees of Animal Care Biosecurity and Bioethics, or by the University of Iowa Animal Use and Care Committee. All personnel were equipped with positive-pressure air-purifying respirators (3M HEPA AirMate, St. Paul, MN).

Construction of pBAC-SARS-CoV-MA15-E* plasmids. Mutant viruses (rSARS-CoV-MA15-E*) with amino acid substitutions in the amino-terminal region (rSARS-CoV-MA15-Mut 1) or with small deletions covering different regions of the carboxy terminus of the E protein (rSARS-CoV-MA15-Δ2, -Δ3, -Δ4, -Δ5, and -Δ6) were constructed using an infectious cDNA clone. cDNA encoding the genome of the SARS-CoV-MA15 strain was assembled in a bacterial artificial chromosome (BAC) (pBAC-SARS-CoV-MA15 plasmid) (32, 58). DNA fragments containing nucleotides (nt) 26044 to 26779 of the SARS-CoV genome were generated by overlap extension PCR in the case of the carboxy-terminal mutants, using as the template the pBAC-SARS-CoV-MA15 plasmid and the primers indicated in Table 1, and by gene synthesis (Bio Basic, Inc.) in the case of the amino-terminal mutant. This last fragment included four point mutations, generating four amino acid changes: S3A (TCA to GCA), V5L (GTT to CTT), T9A (ACA to GCA), and T11A (ACG to GCG). The final PCR products or the fragments generated by gene synthesis were digested with the enzymes BamHI and MfeI and cloned into the intermediate plasmid psl1190+BamHI/SacII SARS-CoV to generate plasmids psl1190+BamHI/SacII SARS-CoV-E* (psl1190-Mut 1, Δ2, Δ3, Δ4, Δ5, and Δ6). Plasmid psl1190+BamHI/SacII SARS-CoV contains a fragment corresponding to nucleotides 26045 to 30091 of the SARS-CoV infectious cDNA clone (59) engineered into the psl1190 plasmid (Pharmacia) using unique BamHI and SacII restriction sites. Finally, these fragments were

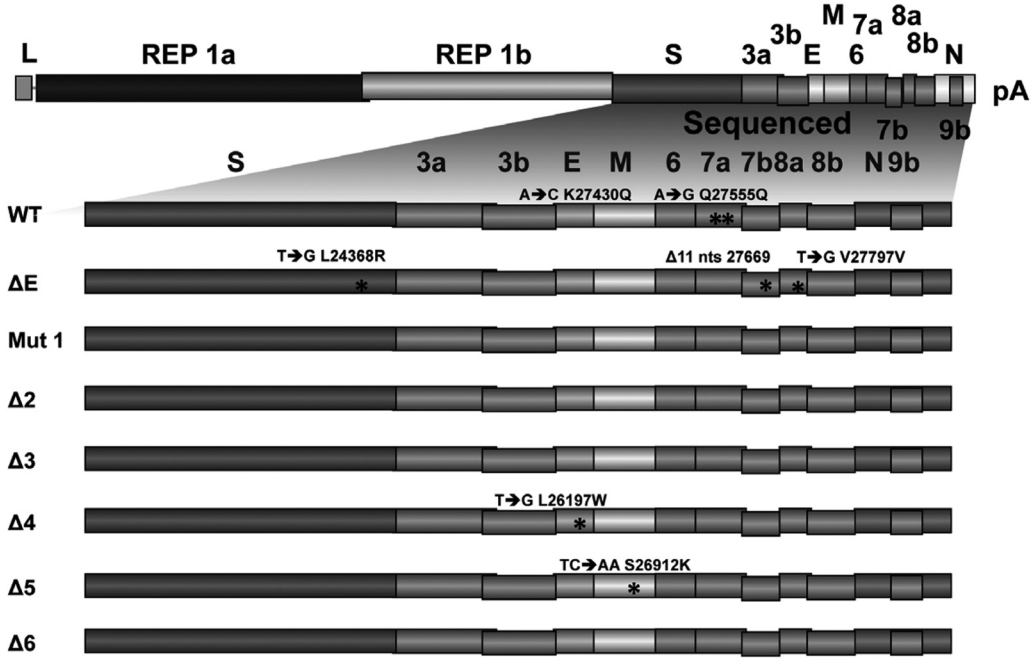

FIG 3 Stability of rSARS-CoV-MA15-E* after serial infections. The stability of rSARS-CoV-MA15-E* virus deletion mutants was examined after 8 passages in Vero E6 cells by sequence analysis. Asterisks denote the presence of nucleotide substitutions.

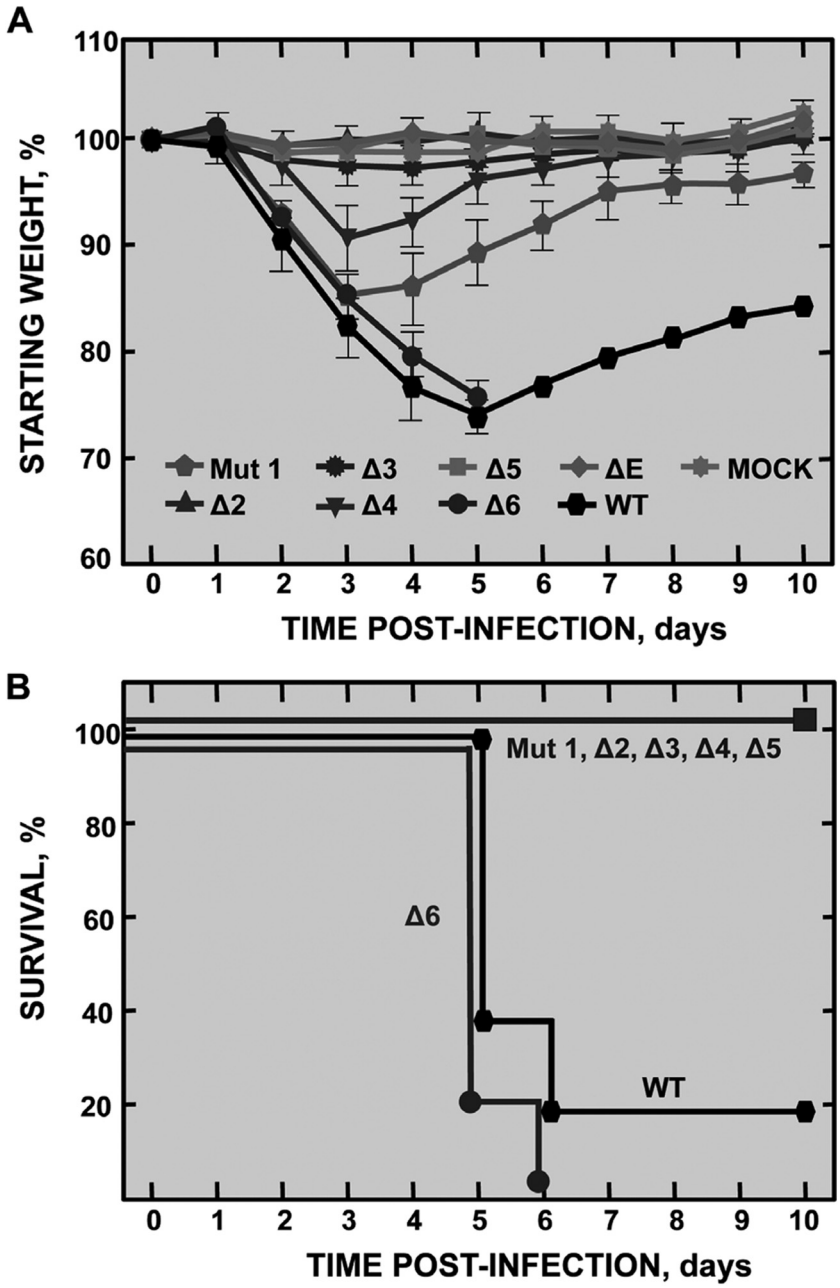

FIG 4 Weight loss and survival rate of mice inoculated with rSARS-CoV-MA15-E* mutants. BALB/c mice were intranasally infected with 1×10^5 PFU of each virus ($n = 5$ mice). Animals were monitored daily for weight loss (A) and survival (B). Animals that lost more than 30% of their initial body weight were euthanized. Differences in weight loss between attenuated and virulent viruses were statistically significant (*, $P < 0.05$).

inserted into pBAC-SARS-CoV-MA15 to generate pBAC-SARS-CoV-MA15-E* plasmids. The viruses were rescued in BHK and Vero E6 cells as previously described (28). Virus was cloned by three rounds of plaque purification.

rSARS-CoV-MA15-E* growth kinetics. Subconfluent monolayers (90% confluence) of Vero E6 or Huh7.5.1 cells were infected at a multiplicity of infection (MOI) of 0.001 with rSARS-CoV-MA15-E*, rSARS-CoV-MA15-ΔE, or rSARS-CoV-MA15. Culture supernatants were collected at the indicated times postinfection, and titers were determined on Vero E6 cells as previously described (28).

Indirect immunofluorescence microscopy. To detect viral E protein expression, Vero E6 cells were grown to 70% confluence on glass coverslips and infected with rSARS-CoV-MA15, rSARS-CoV-MA15-ΔE, and rSARS-CoV-MA15-E* at an MOI of 0.3. At 24 h postinfection (hpi), cells were fixed with 4% paraformaldehyde for 20 min at room temperature. After washing and permeabilization, primary antibody incubations were performed for 90 min at room temperature. Rabbit polyclonal antibody (Ab) specific for E protein (dilution of 1:500; kindly provided by Shen Shuo, Institute of Molecular and Cellular Biology, Singapore) and a mouse anti-ERGIC marker (dilution of 1:200; Alexis Biochemicals) were used. Secondary antibodies specific for rabbit or mice species conjugated to Alexa 488 (for detection of E protein) or Alexa 594 (for detection of ERGIC), respectively (dilution of 1:500; Invitrogen), were incubated for 45 min at room temperature. Nuclei were stained using 4′,6-diamidino-

2-phenylindole (DAPI) (dilution of 1:200; Sigma), and slides were examined on a Leica SP5 confocal microscope (Leica Microsystems).

Specific infectivity of rSARS-CoV-MA15-E* mutants. Subconfluent monolayers (90% confluence) of Vero E6 cells were infected at an MOI of 0.3 with rSARS-CoV-MA15-E*, rSARS-CoV-MA15-ΔE, or rSARS-CoV-MA15. At 8 hpi, the culture medium was harvested and replaced with fresh medium supplemented with 2% fetal bovine serum (FBS). Culture supernatants were collected at 11 hpi ("nascent virus"), and virus titer was determined on Vero E6 cells. Viral RNA was isolated from 400 μl of supernatants using a MagMAX viral RNA isolation kit (Life Technologies) according to the manufacturer's instructions, and genomic RNA was quantified by reverse transcription-quantitative PCR (RT-qPCR) analysis. cDNAs were generated using a high-capacity cDNA transcription kit (Applied Biosystems) and the reverse primer Q-SARS-2015-RS (5′-ATG GCGTCGACAAGACGTAAT-3′). The cDNAs were amplified by qPCR using SYBR green PCR master mix (Applied Biosystems) with forward primer Q-SARS-1931-VS (5′-ACCACTCAATTCCTGATTTGCA-3′) and Q-SARS-2015-RS. The ratio of infectious virus titer to genomic RNA represents the specific infectivity.

Cycloheximide chase to estimate the half-life of rSARS-CoV-MA15-E* mutants. Subconfluent monolayers (90% confluence) of Vero E6 cells were infected with the wt or rSARS-CoV-MA15-E* virus at an MOI of 0.3. At 12 hpi, the cells were treated with 200 μg/ml cycloheximide (Sigma). Cells were harvested at 0, 2, 4, 6, and 8 h, and cell extracts were prepared as previously described (60). Samples were analyzed by sodium dodecyl sulfate-polyacrylamide gel electrophoresis (SDS-PAGE) and Western blotting. In fact, E protein half-life measurements were obtained by calculating E protein relative mass normalized to actin mass for each time point.

Western blot analysis. Cell lysates were resolved by SDS-PAGE, transferred to a nitrocellulose membrane by wet immunotransfer, and processed for Western blotting. The blots were probed with a rabbit polyclonal Ab specific for E protein (dilution of 1:6,000; kindly provided by Shen Shuo, Institute of Molecular and Cellular Biology, Singapore), a monoclonal Ab specific for hemagglutinin (HA) tag (dilution of 1:1,000; Sigma), or an antibody specific for β-actin (dilution of 1:10,000; Abcam). Bound antibodies were detected with horseradish peroxidase-conjugated goat anti-rabbit or anti-mouse antibodies (dilution of 1:30,000; Cappel) and the Immobilon Western chemiluminescent substrate (Millipore). The blots were quantitated by phosphorimaging. The half-life of each E protein mutant was calculated by plotting the signal intensity (ratio of band intensity).

Plasmids. The pcDNA3-E plasmid encoding SARS-CoV E protein was used as previously described (25). To construct a pcDNA3 plasmid encoding the viral M protein fused to an HA tag (pcDNA3-HA-M), primers M-EcoRI-HA-VS (5′-GCGCGCGCGAATTCGCCGCCATGTACCC ATACGATGTTCCAGATTACGCTGCAGACAACGGTACTATTACCG TTGAG-3′, encoding an HA sequence) and M-XhoI-RS (5′-CGCGCTC GAGTTACTGTACTAGCAAAGCAATATTGTC-3′) were used. GAATTC and CTCGAG are the recognition sequences for EcoRI and XhoI, respectively. A DNA fragment encoding the SARS-CoV M protein was generated using as the template the plasmid pBAC-SARS-CoV-MA15. To generate pcDNA3 plasmids encoding the E protein with deletions (pcDNA3-E-Δ3), primers Δ-EcoRI-VS (5′-GCGCGCGCGAATTCGCCGCCATGTA CTCATTCGTTTCGGAAGAAACAG-3′) and Δ-XhoI-RS (5′-CGCGCTCGAGTTAGACCAGAAGATCAGGAACTCCTTCAGAA GAGTT-3′) were used to amplify the DNA fragment encoding the SARS-CoV E deletion proteins using as the template plasmids pBAC-SARS-CoV-MA15-E* with the appropriate deletion. After PCR, these DNA fragments were digested by restriction enzymes EcoRI and XhoI and cloned into pcDNA3-E. All expression plasmids were verified by sequencing.

Immunoprecipitation assay. Vero E6 cells were grown to 90% confluence and cotransfected with a plasmid encoding an N-terminal HA-tagged M protein (pcDNA3-HA-M), combined with plasmids expressing the full-length E protein or E protein with small deletions (pcDNA3-E or pcDNA-E-Δ3). Cells cotransfected with the plasmid pcDNA3-HA-M and the empty plasmid pcDNA3, lacking the coding region of E protein, were used as controls. Twenty-four hours later, cell extracts were collected as previously described (60). For immunoprecipitation assays, monoclonal anti-HA agarose-conjugated clone HA-7 (Sigma) was used by following the manufacturer's instructions. Briefly, 75 μl of the anti-HA agarose conjugate was incubated with the cell extracts overnight at 4°C. Immune complexes were eluted using 20 μl 2× SDS sample buffer and heating at 95°C for 3 min. Analysis of precipitated complexes was carried out by SDS-PAGE and Western blotting.

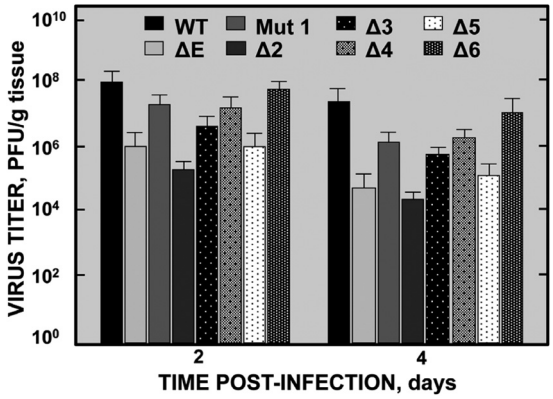

FIG 5 rSARS-CoV-MA15-E* growth in the lungs of infected mice. BALB/c mice were intranasally inoculated with 1×10^5 PFU of the indicated viruses. At 2 and 4 days p.i., lung tissue was harvested and viral titers were analyzed in Vero E6 cell monolayers. Means and standard deviations are shown ($n = 3$ mice).

Virus infection and titration in mice. BALB/c mice were anesthetized with isoflurane and intranasally inoculated with 1×10^5 PFU of virus in 50 μl of Dulbecco's modified Eagle's medium (DMEM). For protection experiments, mice were immunized intranasally with 6×10^3 PFU of the attenuated viruses and then challenged with an intranasal inoculation of 1×10^5 PFU of rSARS-CoV-MA15 at 21 days postimmunization. Mice were monitored daily for weight loss and mortality. SARS-CoV-MA15 titers were measured in Vero E6 cells as described above. Viral titers were expressed as PFU/g tissue.

Histopathologic examination of infected mouse lungs. Lungs were removed from infected mice, fixed in zinc formalin, and paraffin embedded. Sections were stained with hematoxylin and eosin.

RNA analysis by RT-qPCR. BALB/c mice were intranasally inoculated with 1×10^5 PFU of the corresponding virus or DMEM, as a control. Lungs were removed and incubated in RNAlater (Ambion) at 4°C for 24 h, prior to freezing at −80°C. Total RNA was extracted using an RNeasy minikit (Qiagen). Reverse transcription (RT) reactions were performed at 37°C for 2 h using the high-capacity cDNA transcription kit (Applied Biosystems) to generate cDNAs. qPCRs were performed using TaqMan gene expression assays (Applied Biosystems) specific for murine genes (Table 2). Quantification was achieved using the $2^{-\Delta\Delta CT}$ method (61). The data represent the average of duplicate measurements from three independent mice.

Microarray analysis. Lungs from infected mice were collected at 2 days postinfection (p.i.), and total RNA was extracted using an RNeasy minikit (Qiagen). Total RNA from three different lungs was independently hybridized for each transcriptomic comparison. A total of 200 ng of RNA was amplified using a one-color low-input Quick Amp labeling kit (Agilent Technologies) and further purified with an RNeasy minikit (Qiagen). Preparation of probes and hybridization were performed as described in *One-Color Microarray-Based Gene Expression Analysis*, version 6.5 (62). Images were captured with an Agilent microarray scanner, and spots were quantified using feature extraction software (Agilent Tech-

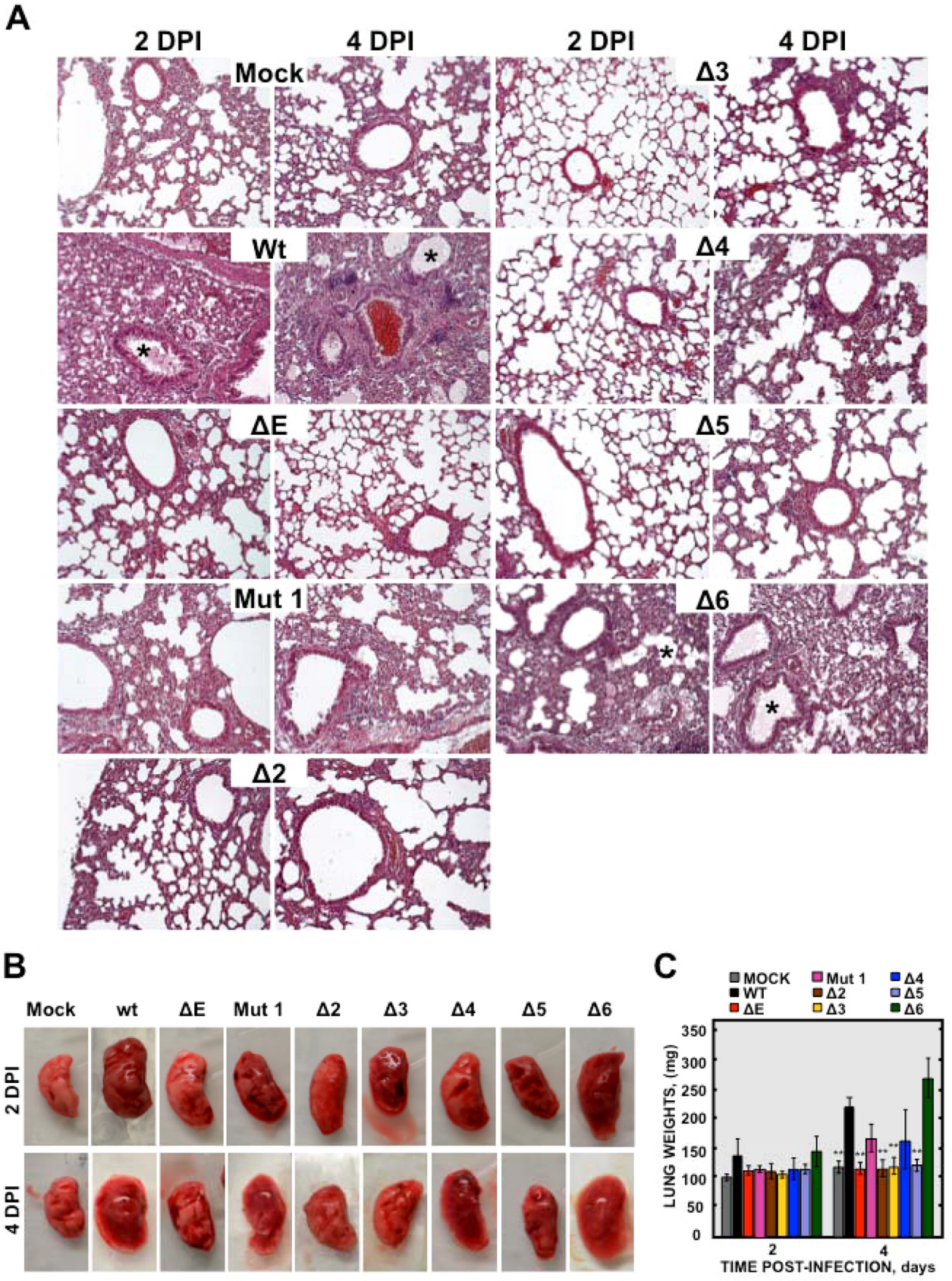

FIG 6 Lung pathology caused by infection with rSARS-CoV-MA15-E* mutants. BALB/c mice were intranasally inoculated with 1×10^5 PFU of the indicated SARS-CoV deletion mutants and sacrificed at days 2 and 4 p.i. (A) Lungs were removed and sections were prepared and stained with hematoxylin and eosin. Asterisks indicate edema accumulation in both bronchiolar and alveolar airways. Original magnification was ×20. Representative images are shown. (B) Macroscopic lung pathology in rSARS-CoV-MA15-E*-infected mice. Representative images of lung gross pathology. (C) Lung weight. Three lungs were evaluated in each case ($n = 3$ mice). Statistically significant data compared to mice infected with the wt virus are indicated (**, $P < 0.01$).

nologies). Background correction and normalization of expression data were performed using linear models for microarray data (LIMMA) (63).

Microarray data analysis. Linear model methods were used for determining differentially expressed genes. Each probe was tested for changes in expression over replicates by using an empirical Bayes moderated *t* statistic (64). To control the false discovery rate (FDR), *P* values were corrected by using the method of Benjamini and Hochberg (64). The expected false discovery rate was controlled to be less than 5%. Genes were considered differentially expressed when the FDRs were <0.05 and fold changes were >2 or <-2.

Measurement of leukocytes in the mouse lungs. Sixteen-week-old BALB/c mice were infected as indicated above with 1×10^5 PFU of each virus. Lungs were removed from mice at 4 days p.i., and cells were prepared as previously described (51). The numbers of macrophages, neutrophils, and CD4 and CD8 T cells were determined as previously described (32, 58).

Cytokine multiplex analysis. Lungs from infected mice were homogenized and nuclear, cytoplasmic, and extracellular proteins were extracted using a nuclear extract kit (Active Motif, Carlsbad, CA). Supernatant proteins (cytoplasmic and extracellular proteins) were diluted 1:5 in assay diluent (Millipore) prior to analysis. The expression of tumor necrosis factor (TNF), MCP-1/CCL2, KC/CXCL1, IL-5, IL-6, IL-13, IFN-γ, macrophage inflammatory protein 1α (MIP-1α)/CCL3, and MIP-1β/CCL4 was determined as previously described (58).

Statistical analysis. Student's *t* test was used to analyze differences in mean values between groups. All results are expressed as means ± standard errors of the means (SEM). *P* values of <0.05 were considered statistically significant.

Microarray data accession number. MIAME-compliant results of the microarrays have been deposited in the Gene Expression Omnibus database (GEO [National Center for Biotechnology Information], accession code GSE59185).

RESULTS

Generation, growth, and characterization of rSARS-CoV-MA15-E* viruses. To identify the E protein regions responsible for rSARS-CoV-ΔE attenuation, a set of mutant viruses (rSARS-CoV-MA15-E*) were generated (Fig. 1A). In rSARS-CoV-MA15-Mut 1, the E protein amino-terminal region was modified by introducing point mutations, instead of deleting amino acids, in order to maintain unaltered the primary sequence of the 3b protein, as 3b and E genes partially overlap. Sequential or partially overlapping small deletions of 6 to 12 amino acids were introduced in the carboxy-terminal region of E protein to generate rSARS-CoV-MA15-Δ2, -Δ3, -Δ4, -Δ5, and -Δ6. The engineered viruses were rescued in Vero E6 cells, cloned by three rounds of plaque purification, and sequenced to confirm the presence of the desired mutations. Mutant E* and wt proteins were similarly localized within infected cells as determined by immunofluorescence by using antibodies specific for the E protein (Fig. 2 and data not shown). All the mutant E proteins partially colocalized with the ERGIC marker as previously observed for the full-length protein (25). These data indicated that none of the regions deleted were essential for the subcellular localization of E protein and that E protein functions that were associated with its localization were not affected. SARS-CoV E protein promotes virus production since elimination of the E gene decreases virus growth from 10- to 100-fold, depending on the cell type (28). To delimit E protein regions involved in SARS-CoV production, growth kinetics of rSARS-CoV-MA15-E* were analyzed in Vero E6 and Huh7.5.1-infected cells (Fig. 1B). Maximum viral titers were observed at 48 to 72 hpi in Vero E6 cells and at 72 hpi in Huh7.5.1 cells, for all the viruses. Mut 1 and Δ6 viruses reached peak titers ($>10^7$ PFU/ml) similar to those observed for rSARS-CoV-MA15 in both cell lines. In contrast, the Δ3 and Δ5 viruses grew to lower titers (around 10^6 and 10^5 PFU/ml in Vero E6 and Huh7.5.1 cells, respectively), similar to those observed for virus lacking full-length E protein (ΔE). The Δ4 virus grew to titers intermediate between titers of the wt and ΔE viruses, reaching titers close to 10^7 and 10^6 PFU/ml in Vero E6 and Huh7.5.1 cells, respectively. The Δ2 virus showed the lowest titers (10^5 and 10^4 PFU/ml in Vero E6 and Huh7.5.1 cells, respectively). These data indicated that deletion of SARS-CoV E protein regions 2, 3, and 5 reduced virus growth to the same extent that the deletion of full-length E protein did, suggesting that these regions themselves were essential for E protein function. In a subsequent experiment, we studied the Δ3 and Δ5 viruses, because viruses grew to titers similar to those of rSARS-CoV-MA15-ΔE.

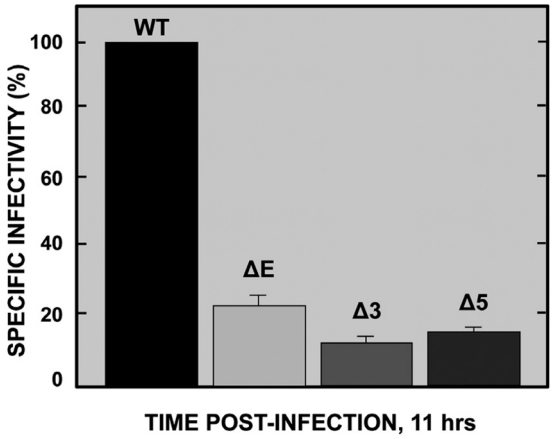

FIG 7 Specific infectivity of rSARS-CoV-MA15-E* mutants. Vero E6 cells were independently infected with each of the rSARS-CoV-MA15-ΔE, -Δ3, and -Δ5 and wt viruses, at an MOI of 0.3. At 8 hpi, the culture medium was harvested and replaced with fresh medium supplemented with 2% FBS. Cell supernatants were collected at 11 hpi ("nascent virus"), and the levels of genomic RNA and infectious virus titer were analyzed by RT-qPCR and plaque assay, respectively. The ratio of infectious virus titer (PFU/ml) to genomic RNA is depicted in the graph as percentage of specific infectivity. Means and standard deviations are shown ($n = 3$ mice).

Stability of rSARS-CoV-MA15-E* mutants in cell cultures. Prior to analyzing the virulence of rSARS-CoV-MA15-E*, their stability in cell culture was examined. The viruses were passaged daily 8 times in Vero E6 cells, followed by sequencing of the distal third of the genome, encompassing the S gene to the 3′ end. Only minor changes were detected in the viral sequences of one representative isolate, suggesting that these viruses were in general genetically stable, at least in tissue culture (Fig. 3). To analyze whether the mutations that the viruses incorporate after growing them in tissue culture cells are compensatory mutations, growth kinetics of the original and passaged viruses were compared by infecting Vero E6 and Huh7.5.1 cells and analyzing virus titers at different times postinfection. No significant differences in the production of infectious viruses were observed among the passaged viruses and the original viruses (data not shown), suggesting that the mutations that the viruses incorporate after growing them in cell culture are not compensatory mutations.

Virulence of rSARS-CoV-MA15-E* mutants. It was previously shown that a SARS-CoV lacking the full-length E protein was fully attenuated *in vivo* (28, 29, 32, 58). To evaluate the relevance of E protein regions in virus virulence, BALB/c mice were

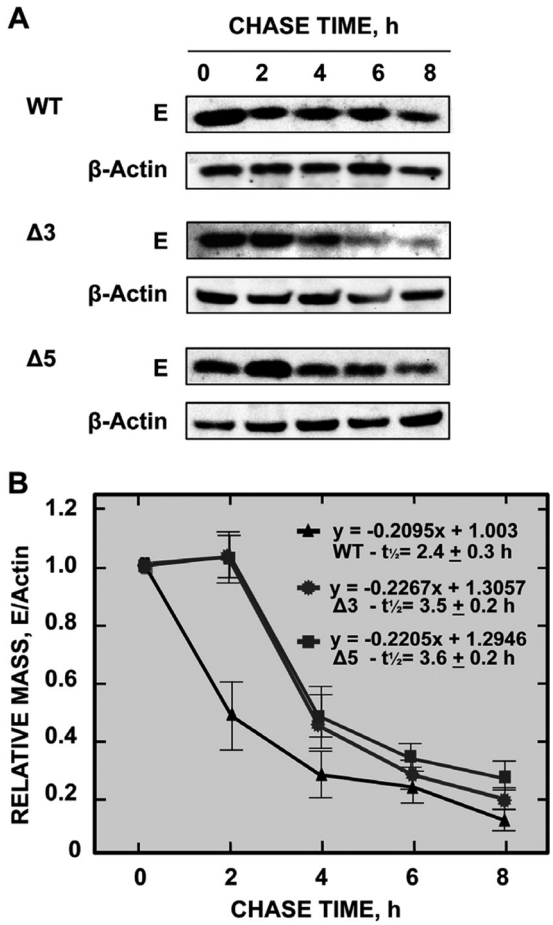

FIG 8 E protein stability of rSARS-CoV-MA15* mutants. Stability of E protein deletion mutants was evaluated in relation to that of the full-length E protein after infection of Vero E6 cells with rSARS-CoV-MA15-E* mutants. At 12 hpi, the cells were treated with cycloheximide. Cells were harvested at the indicated times, and the amount of E protein mutants was determined by Western blotting. (A) Membranes were probed with anti-E protein and with β-actin-specific antibodies as a loading control. (B) The graph represents the values obtained after densitometry analysis. The percentage of protein remaining after cycloheximide addition is represented. Bars represent standard deviations of the mean ($n = 3$ mice).

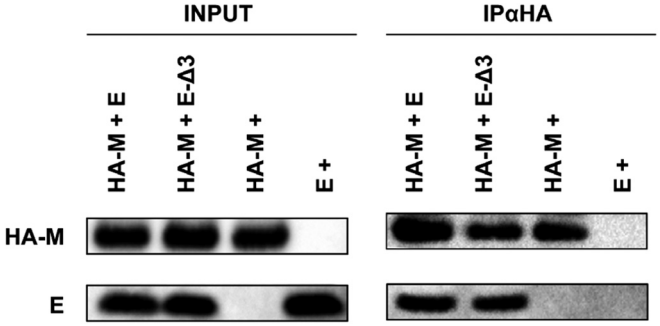

FIG 9 Interaction of SARS-CoV E protein deletion mutants with M protein. Vero E6 cells were cotransfected with a plasmid pcDNA3 encoding the N-terminal HA-tagged M protein, combined with plasmids expressing the E-wt protein or the E protein with a small deletion, E-Δ3. Cotransfections of a plasmid encoding HA-M protein and of a plasmid without E protein were used as controls. Cells were lysed and analyzed by Western blotting with specific antibodies for the E protein and HA (left) or subjected to immunoprecipitation with the monoclonal HA-specific antibody. The presence of E and M proteins was analyzed in the precipitated fractions using E- or HA-specific antibodies (right).

mock infected or infected with rSARS-CoV-MA15-E*, rSARS-CoV-MA15-ΔE, and rSARS-CoV-MA15. Clinical disease and survival were evaluated for 10 days. Mice infected with the parental virus showed disease symptoms from 2 days p.i., reflected by lethargy and ruffled fur. These mice rapidly lost weight, and 80% of them died by day 6 (Fig. 4). Animals infected with Δ6 virus, carrying a deletion in the last segment of the E protein, lost weight and died in a fashion similar to those inoculated with the wild-type virus (Fig. 4). In contrast, mice infected with Δ2, Δ3, Δ5, and ΔE viruses showed no signs of disease (data not shown), did not significantly lose weight, and uniformly survived (Fig. 4). Mice infected with the Mut 1 and Δ4 viruses lost 15% and 10% of their initial weight, respectively, but recovered from 3 days p.i., and all of them survived (Fig. 4). These data showed that E protein regions 1 and 4 and especially 2, 3, and 5 were required to maintain the optimal replication or virulence of SARS-CoV.

rSARS-CoV-MA15-E* growth *in vivo*. To evaluate whether any of the E protein regions were required for optimal virus growth *in vivo*, BALB/c mice were infected with rSARS-CoV-MA15-E*, rSARS-CoV-MA15-ΔE, or rSARS-CoV-MA15, and viral titers in lungs were determined at 2 and 4 days p.i. (Fig. 5). Peak titers were reached by all viruses at 2 days p.i. and decreased around 5- to 20-fold at 4 days p.i. in all cases. The parental virus showed the highest titers, 8×10^7 PFU/g of lung tissue at day 2 and 5×10^7 PFU/g at day 4. Titers were reduced when E protein was fully eliminated (10^6 PFU/g at day 2 and 5×10^4 PFU/g at day 4), confirming that rSARS-CoV-MA15-ΔE replicated less robustly in mice. rSARS-CoV-MA15-Δ6 grew to 7×10^7 PFU/g at 2 days p.i. and 10^7 PFU/g at 4 days p.i., similarly to the wt virus (Fig. 5), indicating that E protein carboxy terminus region 6 is the least relevant for optimal *in vivo* growth. The Δ2 and Δ5 viruses grew to titers similar to those observed for the ΔE virus, or even lower. In contrast, the Mut 1, Δ3, and Δ4 viruses grew to intermediate titers (10^7 PFU/g and 10^6 PFU/g at days 2 and 4, respectively) in lungs. These results are similar to those observed in tissue culture cells and showed that especially regions 2 and 5 of SARS-CoV E protein are required for optimal virus growth.

Lung pathology in rSARS-CoV-MA15-E*-infected mice. To analyze the mechanisms leading to rSARS-CoV-MA15-E* attenuation, macroscopic and microscopic changes in the lungs of infected mice were analyzed at 2 and 4 days p.i. (Fig. 6). The lungs from animals infected with the wt or Δ6 viruses but not ΔE, Mut 1, Δ2, Δ3, Δ4, and Δ5 viruses were increased in volume and were dusky red. Profuse areas of hemorrhage and weight increase, possibly due to leukocyte infiltration and edema accumulation, were especially evident at 4 days p.i. (Fig. 6B and C). In contrast, histological examination of lungs from ΔE, Mut 1, Δ2, Δ3, Δ4, and Δ5 virus-infected mice revealed only a small amount of lung damage and cellular infiltration, whereas examination of lungs infected with wt or Δ6 virus showed substantial lung damage characterized by peribronchial/perivascular inflammatory cell infiltration, edema, and thickening of the alveolar walls at 2 and 4 days p.i. (Fig. 6A). These data demonstrated that E protein regions 1, 2, 3, 4, and 5 contribute to the lung damage induced after SARS-CoV infection.

Specific infectivity and half-life of rSARS-CoV-MA15-E* mutants. In order to investigate whether the different small dele-

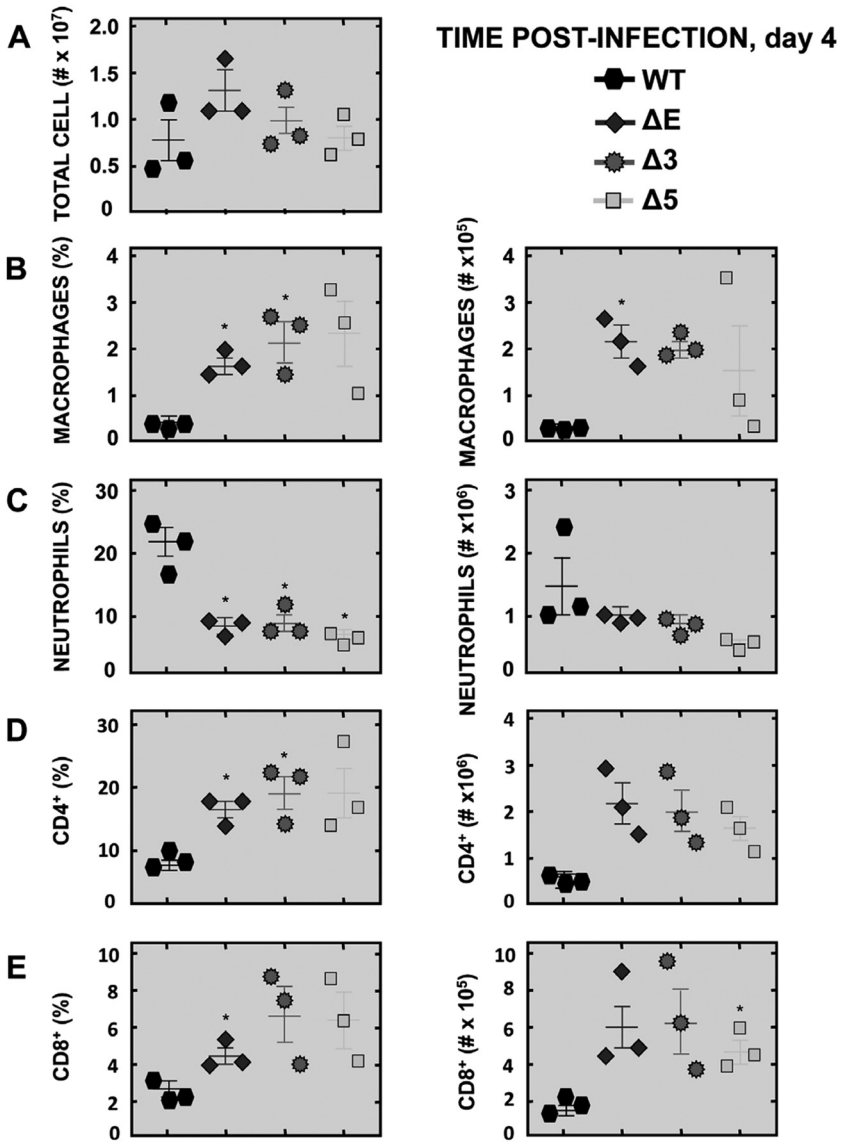

FIG 10 Leukocyte infiltrates present in the lungs of rSARS-CoV-MA15-E*-infected mice. BALB/c mice were intranasally infected with 1×10^5 PFU of the indicated SARS-CoV deletion mutants and sacrificed at 4 days p.i. The total number of leukocytes (A) and total numbers and percentages of macrophages (B), neutrophils (C), $CD4^+$ T cells (D), and $CD8^+$ T cells (E) were determined. Error bars represent the standard deviations of the means. Data are representative of three independent experiments ($n = 3$ mice). Statistically significant differences compared to infection with the wt virus are indicated (*, $P < 0.05$).

tions within the E protein altered virus-specific infectivity, the titers of extracellular rSARS-CoV-MA15-wt, -ΔE, -Δ3, and -Δ5 viruses were compared to the level of the corresponding extracellular genomic RNA. The specific infectivities of rSARS-CoV-MA15-ΔE, -Δ3, and -Δ5 mutants were lower (21%, 11%, and 17%, respectively) than that of the wt virus (Fig. 7). Thus, introducing small deletions or modifications within E protein decreases the infectivity of the particles, probably contributing to the lower titers observed for the rSARS-CoV-MA15-ΔE, -Δ3, and -Δ5 mutants.

To analyze whether the small deletions introduced in the E protein changed its stability, cellular translation was inhibited with cycloheximide, and the degradation of E protein was analyzed by Western blotting. The half-lives of the E proteins encoded by the rSARS-CoV-MA15-Δ3 and -Δ5 virus mutants were longer (3.5 h and 3.6 h, respectively) than that of the wt E protein, which had a half-life of 2.4 h, in agreement with previous results (65) (Fig. 8). The fact that wild-type E protein has a shorter half-life can be explained, because this protein is more abundantly expressed at early times compared to mutant proteins. These results suggest that the introduction of small deletions within the E protein modestly alter the stability of the protein.

Binding between E protein and M protein. The interactions between SARS-CoV E and M proteins play an essential role in the viral particle assembly (66–68). Based on this observation, and on the result showing that the rSARS-CoV-MA15-Δ3 and -Δ5 viruses grew to lower titers than those for wt virus in cell cultures, the interaction between the E-Δ3 deletion protein and the M protein was analyzed. To this end, an HA-tagged, full-length M protein and E-Δ3 deletion protein were coexpressed in Vero E6 cells by

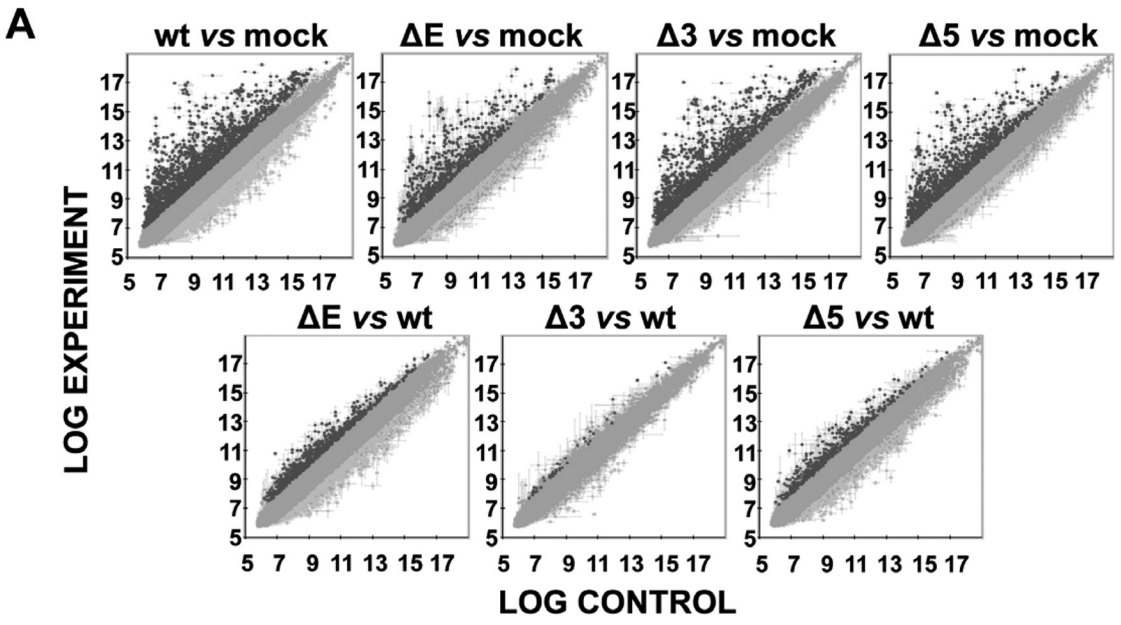

B

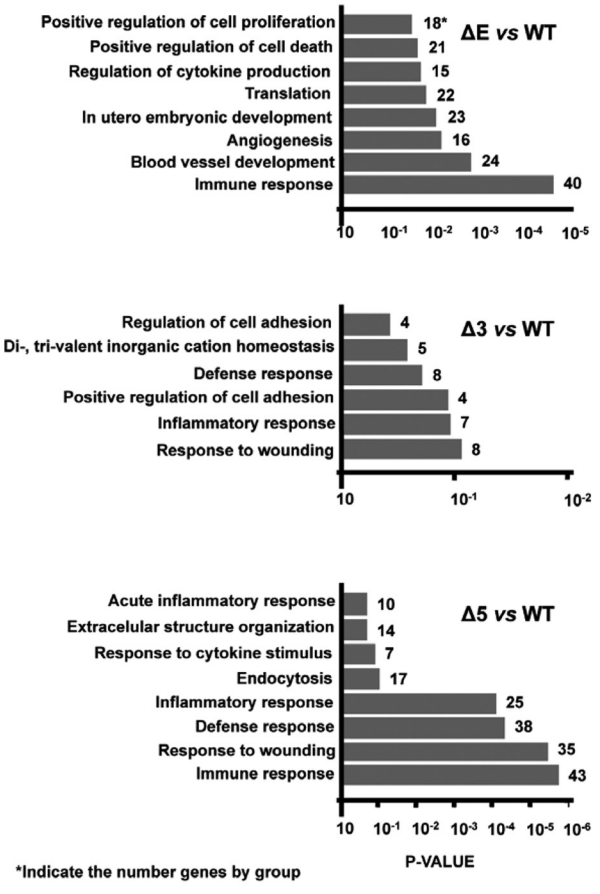

C

GENE	FOLD CHANGE ΔE vs WT	Δ3 vs WT	Δ5 vs WT
INFLAMMATION			
CXCL5 (Ena-78/Lix)	-1.9	-3.9	+1.6
CCL4 (Mip-1b)*	-2.4	-2.6	-1.2
CCL19	-2.8	-2.1	-1.7
CXCL2 (Il8rb)*	-2.8	-2.7	-2.2
CCL3 (Mip-1a)*	-2.9	-3.0	-2.5
NFKB2	-3.2	-1.5	-3.5
CX3CL1	-3.5	-1.2	-2.0
TNF*	-3.4	-2.5	-3.3
CCL2 (Mcp-1)*	-3.8	-2.5	-2.9
CXCL9 (Mig)	-4.7	-3.2	-3.9
CXCL13	-5.9	-2.5	-4.5
IL10	-2.2	-2.1	-2.5
CXCL1 (Il8ra)*	-2.5	-4.8	-2.1
CSF3 (GCSF)	-2.2	-2.1	-2.3
CXCL10 (Inp10)*	-3.1	-1.8	-1.8
PTX3	-4.2	-2.1	-2.5
IL6*	-2.5	-1.8	-1.3
IL4*	+2.7	+1.2	+2.5
IL13*	+2.7	+1.0	+2.7
IMMUNE RESPONSE			
IL5*	+4.4	+1.4	+6.4
IL12B*	-3.9	-2.3	-3.6
IFN RESPONSE			
IFNγ*	-2.7	-2.3	-2.1
IFIH1	-3.0	-1.2	-1.9
MX1	-5.1	-1.5	-2.3
IFNβ	-5.6	-3.1	-2.2
COMPLEMENT ACTIVATION			
C1S	-2.1	+1.1	-2.0
C1QC	-2.1	-1.8	-2.2
SERPING1	-2.3	+1.3	-2.4
C3	-3.0	+1.2	-1.9
CFB	-4.7	-1.1	-3.3
TRANSCRIPTION			
STAT3	-2.6	+1.1	-2.1

FIG 11 Differential gene expression in rSARS-CoV-MA15-E*-infected mice. Total lung RNA was extracted from mice infected with the indicated SARS-CoV deletion mutants at 2 days p.i. ($n = 3$ mice). (A) Differential gene expression was measured using microarrays. Only genes with an FDR less than 0.05 were considered candidate genes. Points with a differential expression higher or lower than 2-fold are represented as darker or lighter dots, respectively. (B) Candidate genes that were up- and downregulated in ΔE, Δ3, and Δ5 viruses were grouped according to Gene Ontology terms. Numbers on the *x* axis indicate DAVID FDR values. (C) Genes differentially expressed in ΔE-, Δ3-, and Δ5-infected mice compared to in wt-infected mice were classified according to their main biological functions. Black and gray lettering is used to indicate up- and downregulated genes, respectively. Asterisks indicates genes whose expression was confirmed by RT-qPCR. The numbers indicate the fold change for each gene in ΔE-, Δ3-, and Δ5-infected mice compared to in wt-infected mice. For those genes detected with more than one probe, the value corresponding to the highest upregulation or downregulation is represented.

TABLE 3 Analysis of host gene expression using mouse microarrays[a]

Comparison	Total no. of genes differentially expressed	No. of upregulated genes	No. of downregulated genes
WT vs mock	2,918	1,473	1,445
ΔE mutant vs mock	957	594	363
Δ3 mutant vs mock	1,466	1,004	462
Δ5 mutant vs mock	1,362	955	409
ΔE mutant vs WT	1,382	752	630
Δ3 mutant vs WT	83	39	44
Δ5 mutant vs WT	286	441	385

[a] Upregulated, fold change of >2, FDR of <0.05; downregulated, fold change of <−2, FDR of <0.05.

transient transfection, and coimmunoprecipitation experiments were performed. The E-wt and E-Δ3 proteins were specifically coimmunoprecipitated together with the M protein, using an antibody specific for the HA tag fused to the M protein (Fig. 9). These results confirm that E and M proteins interacted in infected cells and indicated that the Δ3 deletion introduced within the E protein did not significantly alter the binding of this protein to the M protein.

Immune cell responses in rSARS-CoV-MA15-E*-infected mice. SARS progression and disease outcomes are associated with a massive influx of inflammatory cells to the lungs and a poor T cell response (50, 51, 54, 69). Leukocyte infiltrates in the lungs of mice infected with virulent rSARS-CoV-MA15-wt or representative attenuated mutants (rSARS-CoV-MA15-ΔE, -Δ3, and -Δ5) were quantified and characterized by flow cytometry. Total leukocyte numbers were slightly increased in lung cell infiltrates of mice infected with the attenuated mutants (ΔE, Δ3, and Δ5 viruses), compared to those infected with the parental virulent virus (Fig. 10A). Higher total and relative levels of macrophages were observed in lung infiltrates of the mice infected with the attenuated viruses than in those infected with rSARS-CoV-MA15 (Fig. 10B). Interestingly, a decrease in the percentage and total number of neutrophils was observed in the mice infected with the attenuated viruses compared to those in rSARS-CoV-MA15-infected mice (Fig. 10C). These data showed that the attenuation observed for mutant viruses (ΔE, Δ3, and Δ5 viruses) correlated with a decrease in neutrophil influx and an increase in macrophage influx into the lungs. Higher total and relative numbers of $CD4^+$ and $CD8^+$ T cells were present in the lungs of ΔE, Δ3, and Δ5 virus-infected mice than in virulent rSARS-CoV-MA15-infected lungs (Fig. 10D and E). All data analyzed were statistically significant, with the exception of total leukocyte, neutrophil, and $CD4^+$ numbers. These data suggested that mice infected with the attenuated viruses develop higher T cell responses than those infected with virulent SARS-CoV, most likely contributing to virus clearance and disease attenuation.

Effect of SARS-CoV-MA15-E* virus infection on host gene expression. To analyze host responses responsible for the attenuation of the rSARS-CoV-MA15-E* mutants, the transcriptomes of rSARS-CoV-MA15-, rSARS-CoV-MA15-ΔE-, rSARS-CoV-MA15-Δ3-, rSARS-CoV-MA15-Δ5-, and mock-infected lungs were compared, using mouse microarrays (Fig. 11A and Table 3). The genes differentially expressed during SARS-CoV infection (both up- and downregulated) in rSARS-CoV-MA15-ΔE, -Δ3, and -Δ5 virus-infected mice, compared to wt-infected mice, were clustered using DAVID software (70). The most statistically significant clusters were associated with the immune response, the response to wounding, the defense response, and the inflammatory response (Fig. 11B). Based on their principal biological function, the genes downregulated in mice infected with the attenuated rSARS-CoV-MA15 mutants were involved mainly in inflammation (Fig. 11C). Interestingly, this reduction correlated with relative increase in the expression of the Th2 genes, such as those encoding IL-4 and IL-13, in comparison to that in mice infected with the parental virus.

To validate and confirm the results obtained using microarrays, several genes involved in inflammatory responses were selected for RT-qPCR analysis, and their expression was tested at 2 and 4 days p.i. A clear reduction of all the proinflammatory cytokines analyzed (TNF, CCL2, CCL3, CCL4, CXCL1, CXCL2, CXCL10, IL-6, IL-12B, and IFN-γ) was observed in the lungs of mice infected with the ΔE, Δ3, and Δ5 attenuated viruses, compared to that in wt-infected mouse lungs (Fig. 11C and 12A and B). In contrast, the expression of the Th2 cytokines IL-4, IL-5, and IL-13 was upregulated in the lungs of mice infected with the ΔE, Δ3, and Δ5 attenuated viruses, compared to those from rSARS-CoV-MA15-infected mice (Fig. 11C and 12A and B). All data analyzed were statistically significant with minor exceptions. These changes were specific, as the mRNA levels of rRNA 18S and transforming growth factor β (TGF-β), encoded by another gene involved in the anti-inflammatory response but regulated posttranscriptionally (71, 72), were the same in all mice (Fig. 12B).

To confirm that the mRNA levels correlated with protein accumulation, the levels of TNF, CCL2, CXCL1, IL-5, IL-6, IL-13, IFN-γ, CCL3, and CCL4 were evaluated in lung extracts from mice infected with the rSARS-CoV-MA15, Δ3, Δ5, and ΔE viruses or mock infected, as a control. mRNA levels of these cytokines matched with their protein levels in the mouse lungs (Fig. 13). All cytokine differences at the protein level were statistically significant, with minor exceptions in CCL3, CXCL1, and CCL4 cytokines. All together, these results indicated that the macroscopic and microscopic inflammation present in the lungs of infected mice correlated with overexpression of proinflammatory cytokines and downregulation of anti-inflammatory cytokines.

Immunization with the attenuated mutant viruses protects mice against challenge with SARS-CoV-MA15 virus. Live attenuated vaccines are considered most effective in their ability to induce a long-lived, balanced immune response. In order to determine whether the attenuated mutant viruses were good vaccine candidates, the induction of protection conferred by the attenuated viruses with point mutations or small deletions, against the challenge with virulent SARS-CoV-MA15, was studied. Groups of BALB/c mice were either mock immunized with PBS or immunized with the Mut 1, Δ2, Δ3, Δ4, and Δ5 attenuated viruses. At 21 days postimmunization, mice were challenged with rSARS-CoV-MA15, and weight loss and mortality were monitored for 14 days postchallenge (Fig. 14). All the nonimmunized mice lost weight and died by day 7 after rSARS-CoV-MA15 challenge. In contrast, vaccination with the attenuated mutant viruses completely protected mice from the lethal dose of SARS-CoV-MA15, as they showed no weight loss and all survived. These data indicated that all attenuated mutant viruses effectively induced a high level of protection against lethal rSARS-CoV-MA15 challenge in mice.

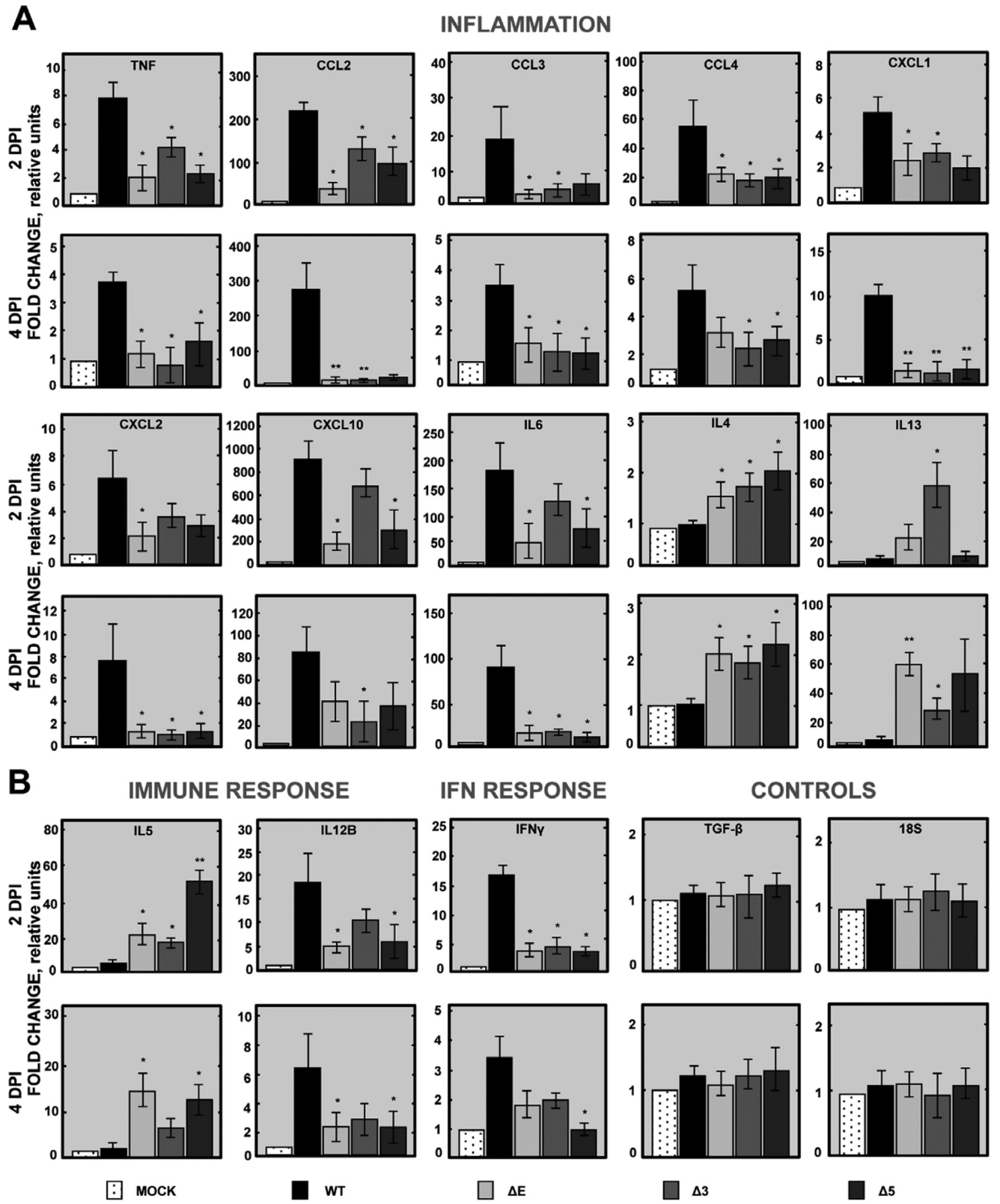

FIG 12 Effect of rSARS-CoV-MA15-E* deletion mutants on the expression of cytokine mRNAs in BALB/c mouse lung. Mice were infected with 1×10^5 PFU of rSARS-CoV-MA15-Δ3, -Δ5, and -ΔE and wt viruses, and total RNA was extracted at 2 and 4 days p.i. The expression of mRNAs encoding inflammatory genes (A) and immune response and IFN response genes encoding TGFβ and 18S rRNA (B) was measured by qRT-PCR. In each case, levels of expression in infected lungs were compared to those in mock-infected ones. Bars represent standard deviations of the mean ($n = 3$ mice). Statistically significant data compared to mice infected with the wt virus are indicated (*, $P < 0.05$; **, $P < 0.01$).

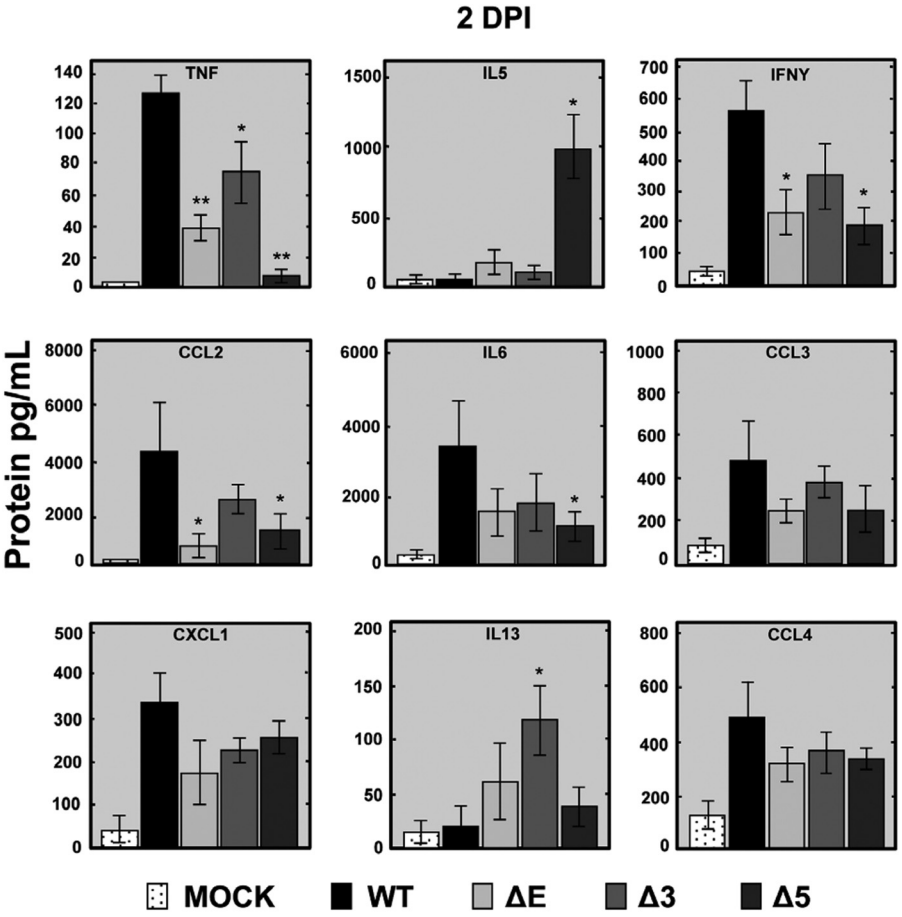

FIG 13 Expression of cytokines in rSARS-CoV-MA15-E*-infected mice. Mice were infected with 1×10^5 PFU of rSARS-CoV-MA15-wt, -Δ3, -Δ5, or -ΔE virus or were mock infected (mock). Lung proteins were extracted at 2 days p.i., and the accumulation of several cytokine proteins was measured. Protein concentration is expressed as picograms per milliliter of lung tissue extract. Means and standard deviations are shown ($n = 3$ mice). Statistically significant differences compared to mice infected with wt virus are indicated (*, $P < 0.05$).

DISCUSSION

An extensive study using a collection of recombinant viruses was performed to analyze E protein regions and host responses that contributed to the virulence of SARS-CoV. Several mutants encoding small deletions or point mutations within E protein were engineered, in the context of mouse-adapted SARS-CoV-MA15 (57). Point mutations in the amino-terminal region and small deletions in the internal carboxy-terminal region of E protein led to viruses with an attenuated phenotype, similarly to that obtained by deleting the whole E protein of SARS-CoV. Infection of mice with the rSARS-CoV-MA15-Mut 1, -Δ2, -Δ3, -Δ4, -Δ5, and -ΔE mutants led to decreased lung pathology compared to that of wt-infected mice and no mortality. Therefore, these regions are required for the virus to develop its full pathogenic potential. In contrast, virus lacking the 12 carboxy-terminal amino acids of E protein (Δ6 mutant) was fully virulent, reinforcing the idea that not all small deletions within the E protein were attenuating. The deletion within rSARS-CoV-MA15-Δ6 includes the PDZ-binding motif (PBM) (73, 74), and we previously showed that a mutant lacking this region is attenuated (73). One possible explanation for this apparent discrepancy is that the last 6 amino acids within the Δ6 virus (YSRVKN; Fig. 1) form an alternative PBM that could restore the virulent phenotype of the virus, an aspect that is currently being explored in our laboratory. Deletion or mutation of E protein regions could in principle affect basic properties of the protein, such as its subcellular localization and half-life, which could broadly disturb its major functions within the cell. The cytoplasmic tail of SARS-CoV E protein was shown to contain a signal providing Golgi localization (75). In addition, CoV E protein may impair protein trafficking depending of its half-life (65). None of these aspects was significantly altered, as mutant E proteins colocalized mainly with ERGIC markers, as described for the wt protein (25), and the half-life of E* protein mutants was slightly increased (1.5-fold) compared with that of the wt protein (65). Furthermore, the interaction between E and M proteins necessary for virus morphogenesis (66–68) was preserved despite deleting the Δ3 region. Thus, the E-Δ3 region of SARS-CoV E protein is not required to interact with M protein. In contrast, the specific infectivity of the different small deletions within the E protein was lower (6-fold) than that of the wt virus. These modifications in E protein possibly contributed to the reduced infectivity observed for E protein deletion mutants that exhibited an attenuated phenotype. However, these phenomena are not necessarily linked, because we previously demonstrated that recombinant viruses containing point mutations in the E protein that inhibited its ion channel activity or eliminated its PBM grew to titers similar to

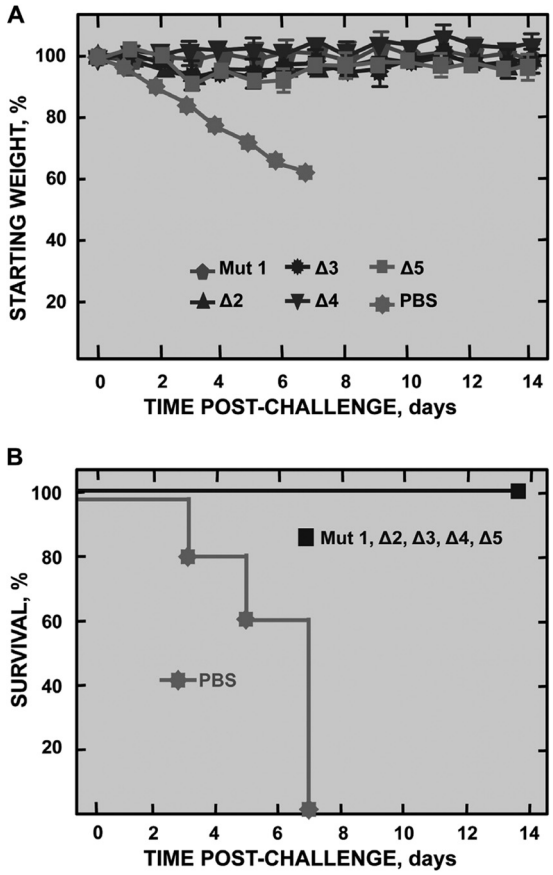

FIG 14 Protection conferred by immunization with the rSARS-CoV-MA15-E* mutants. Six-week-old BALB/c mice were mock immunized or immunized with 6,000 PFU of the SARS-CoV-MA15-E* mutants and challenged at day 21 postimmunization with 1×10^5 PFU of MA15 virus ($n = 5$ mice). Weight loss (A) and survival (B) were recorded daily.

those of the parental virus in the lungs of the infected mice (37, 73). Nevertheless, these viruses caused a reduction in lung inflammation and pathology and were attenuated (37, 73). Therefore, E* protein mutants may decrease virus virulence by affecting specific host responses, independently of effects on virus replication. Interestingly, the patterns of gene expression in infected lungs revealed that proinflammatory genes, such as those encoding TNF, CCL2, CCL3, CCL4, CXCL1, CXCL2, CXCL10, IL-6, IL-12B, and IFN-γ, were downregulated in rSARS-CoV-MA15-ΔE, -Δ3, and -Δ5-infected mice compared to in wt-infected mice, most probably contributing to viral attenuation. Notably, increased levels of proinflammatory cytokines such as TNF, IL-6, CXCL10, CCL2, IL-8, and IL-12, which play a major role in mediating and amplifying ALI/ARDS, were found in the blood and the lungs of SARS patients (40–45, 48, 76). Furthermore, the expression of the Th2 cytokines IL-4, IL-5, and IL-13 was increased in the lungs of mice infected with the attenuated viruses compared to in those infected with the virulent wt virus, possibly contributing to a better outcome. In agreement with this finding, the expression of IL-13 was increased in asymptomatic young BALB/c mice infected with a mouse-adapted SARS-CoV, compared to aged infected mice with severe respiratory disease (77). All these data strongly suggest that the lower proinflammatory cytokine expression and higher anti-inflammatory cytokine levels observed after infection with the attenuated mutants could account for the diminished lung pathology and virus attenuation.

Neutrophils play a key role in the progression of ALI/ARDS, and SARS patients with adverse outcomes presented with neutrophilia and high neutrophil counts in the lungs (38, 54, 78, 79). Similarly, massive neutrophil influx into the lungs contributed to disease after influenza A virus and respiratory syncytial virus (RSV) infections (80–83). This phenomenon was reproduced in mice infected with virulent SARS-CoV-MA15, whereas a significant reduction of neutrophils in the lungs of the mice infected with the attenuated mutants was observed. Accordingly, the expression of CXCL1 and CXCL2, key factors that induce the chemotaxis of neutrophils (84, 85), was increased when the full-length E protein was present during SARS-CoV infection.

An increase of macrophage numbers was observed in mice infected with the attenuated mutants, compared to those infected with the virulent wt virus. In addition to their role in immunity, macrophages maintain physiologic homeostasis and contribute to tissue repair (86, 87). Therefore, an increase of these cells during infection could favor disease resolution. Together, these data indicate that an increase in neutrophil numbers in conjunction with a decrease in macrophage numbers in the lungs is associated with more severe SARS-CoV pathogenesis and that the deletion of E protein carboxy-terminal regions was responsible for these changes in the phenotype of infiltrating immune cells and virus attenuation during SARS-CoV infection.

T cells are important for viral clearance and for protection from disease in primary SARS-CoV infection (50–52), and low T cell counts correlate with adverse outcomes in SARS patients (38, 53, 54, 56). Interestingly, we have shown that in rSARS-CoV-MA15-ΔE, -Δ3, and -Δ5-infected mice, which do not show a significant disease, $CD4^+$ and $CD8^+$ T cell counts are higher than those found in mice infected with the parental virus, which show adverse outcomes after infection. We were unable to measure virus-specific T cell responses, because rSARS-CoV-infected mice die before a significant T cell response develops (Fig. 4). Several anti-SARS-CoV vaccine candidates have been developed since 2003, but none has been approved for use in humans (88, 89). Live attenuated vaccines are considered most effective compared to other types of vaccines, as they induce a long-lived, balanced immune response. Remarkably, the attenuated mutants generated in this work provided full protection after challenge with the virulent wt virus. These viruses express a complete repertoire of viral proteins, except for the small regions deleted or mutated in the E protein. Therefore, it is predicted that they will elicit both antibody and T cell responses directed against the virus. The major problems of using live attenuated vaccines are the possibility that the viruses may revert to virulence. To overcome this limitation, we are introducing additional attenuating mutations into the Nsp1 protein to generate a safer vaccine candidate. The Nsp1 gene was selected as a target because it is located at a very distant site from that of the E gene in the viral genome, making the generation of a virulent virus through single recombination events with circulating coronaviruses unlikely.

In summary, we have shown that changes in the amino terminal and internal carboxy-terminal regions of E protein led to stable attenuated SARS-CoV mutants. These mutants showed a slight reduction in their specific infectivity, maintained the same E protein subcellular localization, and slightly increased their half-

life compared to the wild-type virus. Moreover, the Δ3 deletion introduced within the E protein maintained the interaction between E and M proteins. SARS-CoV attenuation correlated with limited lung pathology, mediated by decreased proinflammatory cytokine expression, increased anti-inflammatory cytokine levels, and reduced neutrophil accumulation in the lungs. In addition, higher $CD4^+$ and $CD8^+$ T cell counts in mice infected with the attenuated mutants most likely contributed to better outcomes. These attenuated mutants fully protected mice from challenge with virulent virus. These studies are the basis for the rational design of SARS-CoV vaccine candidates.

ACKNOWLEDGMENTS

This work was supported by grants from the Ministry of Science and Innovation of Spain (MICINN BIO2010-16705 and MINECO BIO2013-42869-R), the European Community's Seventh Framework Programme (FP7/2007–2013) under the project "EMPERIE" EC grant agreement number 223498, and a U.S. National Institutes of Health (NIH) project (2P01AI060699). J.A.R.-N. and C.C.-R. received a fellowship from the Fundacion La Caixa.

We thank Marga Gonzalez for her technical assistance.

REFERENCES

1. **Perlman S, Netland J.** 2009. Coronaviruses post-SARS: update on replication and pathogenesis. Nat Rev Microbiol **7:**439–450. http://dx.doi.org/10.1038/nrmicro2147.
2. **Drosten C, Gunther S, Preiser W, van der Werf S, Brodt HR, Becker S, Rabenau H, Panning M, Kolesnikova L, Fouchier RA, Berger A, Burguiere AM, Cinatl J, Eickmann M, Escriou N, Grywna K, Kramme S, Manuguerra JC, Muller S, Rickerts V, Sturmer M, Vieth S, Klenk HD, Osterhaus AD, Schmitz H, Doerr HW.** 2003. Identification of a novel coronavirus in patients with severe acute respiratory syndrome. N Engl J Med **348:**1967–1976. http://dx.doi.org/10.1056/NEJMoa030747.
3. **Rota PA, Oberste MS, Monroe SS, Nix WA, Campganoli R, Icenogle JP, Peñaranda S, Bankamp B, Maher K, Chen M-H, Tong S, Tamin A, Lowe L, Frace M, DeRisi JL, Chen Q, Wang D, Erdman DD, Peret TC, Burns C, Ksiazek TG, Rollin PE, Sanchez A, Liffick S, Holloway B, Limor J, McCaustland K, Olsen-Rassmussen M, Fouchier R, Gunther S, Osterhaus AD, Drosten C, Pallansch MA, Anderson LJ, Bellini WJ.** 2003. Characterization of a novel coronavirus associated with severe acute respiratory syndrome. Science **300:**1394–1399. http://dx.doi.org/10.1126/science.1085952.
4. **Kuiken T, Fouchier RAM, Schutten M, Rimmelzwaan GF, van Amerongen G, van Riel D, Laman JD, de Jong T, van Doornum G, Lim W, Ling AE, Chan PKS, Tam JS, Zambon MC, Gopal R, Drosten C, van der Werf S, Escriou N, Manuguerra J-C, Stohr K, Peiris JSM.** 2003. Newly discovered coronavirus as the primary cause of severe acute respiratory syndrome. Lancet **362:**263–270. http://dx.doi.org/10.1016/S0140-6736(03)13967-0.
5. **Marra MA, Jones SJM, Astell CR, Holt RA, Brooks-Wilson A, Butterfield YSN, Khattra J, Asano JK, Barber SA, Chan SY, Cloutier A, Coughlin SM, Freeman D, Girn N, Griffith OL, Leach SR, Mayo M, McDonald H, Montgomery SB, Pandoh PK, Petrescu AS, Robertson AG, Schein JE, Siddiqui A, Smailus DE, Stott JM, Yang GS, Plummer F, Andonov A, Artsob H, Bastien N, Bernard K, Booth TF, Bowness D, Czub M, Drebot M, Fernando L, Flick R, Garbutt M, Gray M, Grolla A, Jones S, Feldmann H, Meyers A, Kabani A, Li Y, Normand S, Stroher U, Tipples GA, Tyler S, et al.** 2003. The genome sequence of the SARS-associated coronavirus. Science **300:**1399–1404. http://dx.doi.org/10.1126/science.1085953.
6. **Zaki AM, van Boheemen S, Bestebroer TM, Osterhaus AD, Fouchier RA.** 2012. Isolation of a novel coronavirus from a man with pneumonia in Saudi Arabia. N Engl J Med **367:**1814–1820. http://dx.doi.org/10.1056/NEJMoa1211721.
7. **de Groot RJ, Baker SC, Baric RS, Brown CS, Drosten C, Enjuanes L, Fouchier RA, Galiano M, Gorbalenya AE, Memish ZA, Perlman S, Poon LL, Snijder EJ, Stephens GM, Woo PC, Zaki AM, Zambon M, Ziebuhr J.** 2013. Middle East respiratory syndrome coronavirus (MERS-CoV): announcement of the Coronavirus Study Group. J Virol **87:**7790–7792. http://dx.doi.org/10.1128/JVI.01244-13.
8. **WHO.** 2013. Middle East respiratory syndrome coronavirus (MERS-CoV)—update. WHO, Geneva, Switzerland. http://www.who.int/csr/don/2013_08_01/en/index.html.
9. **van Boheemen S, de Graaf M, Lauber C, Bestebroer TM, Raj VS, Zaki AM, Osterhaus AD, Haagmans BL, Gorbalenya AE, Snijder EJ, Fouchier RA.** 2012. Genomic characterization of a newly discovered coronavirus associated with acute respiratory distress syndrome in humans. mBio **3**(6):e00473–12. http://dx.doi.org/10.1128/mBio.00473-12.
10. **Muller MA, Paweska JT, Leman PA, Drosten C, Grywna K, Kemp A, Braack L, Sonnenberg K, Niedrig M, Swanepoel R.** 2007. Coronavirus antibodies in African bat species. Emerg Infect Dis **13:**1367–1370. http://dx.doi.org/10.3201/eid1309.070342.
11. **Chu DK, Peiris JS, Chen H, Guan Y, Poon LL.** 2008. Genomic characterizations of bat coronaviruses (1A, 1B and HKU8) and evidence for co-infections in Miniopterus bats. J Gen Virol **89:**1282–1287. http://dx.doi.org/10.1099/vir.0.83605-0.
12. **Drexler JF, Gloza-Rausch F, Glende J, Corman VM, Muth D, Goettsche M, Seebens A, Niedrig M, Pfefferle S, Yordanov S, Zhelyazkov L, Hermanns U, Vallo P, Lukashev A, Muller MA, Deng H, Herrler G, Drosten C.** 2010. Genomic characterization of severe acute respiratory syndrome-related coronavirus in European bats and classification of coronaviruses based on partial RNA-dependent RNA polymerase gene sequences. J Virol **84:**11336–11349. http://dx.doi.org/10.1128/JVI.00650-10.
13. **Quan PL, Firth C, Street C, Henriquez JA, Petrosov A, Tashmukhamedova A, Hutchison SK, Egholm M, Osinubi MO, Niezgoda M, Ogunkoya AB, Briese T, Rupprecht CE, Lipkin WI.** 2010. Identification of a severe acute respiratory syndrome coronavirus-like virus in a leaf-nosed bat in Nigeria. mBio **1**(4):e00208–10. http://dx.doi.org/10.1128/mBio.00208-10.
14. **Annan A, Baldwin HJ, Corman VM, Klose SM, Owusu M, Nkrumah EE, Badu EK, Anti P, Agbenyega O, Meyer B, Oppong S, Sarkodie YA, Kalko EK, Lina PH, Godlevska EV, Reusken C, Seebens A, Gloza-Rausch F, Vallo P, Tschapka M, Drosten C, Drexler JF.** 2013. Human betacoronavirus 2c EMC/2012-related viruses in bats, Ghana and Europe. Emerg Infect Dis **19:**456–459. http://dx.doi.org/10.3201/eid1903.121503.
15. **Falcon A, Vazquez-Moron S, Casas I, Aznar C, Ruiz G, Pozo F, Perez-Brena P, Juste J, Ibanez C, Garin I, Aihartza J, Echevarria JE.** 2011. Detection of alpha and betacoronaviruses in multiple Iberian bat species. Arch Virol **156:**1883–1890. http://dx.doi.org/10.1007/s00705-011-1057-1.
16. **Gorbalenya AE, Snijder EJ, Spaan WJ.** 2004. Severe acute respiratory syndrome coronavirus phylogeny: toward consensus. J Virol **78:**7863–7866. http://dx.doi.org/10.1128/JVI.78.15.7863-7866.2004.
17. **Snijder EJ, Bredenbeek PJ, Dobbe JC, Thiel V, Ziebuhr J, Poon LLM, Guan Y, Rozanov M, Spaan WJM, Gorbalenya AE.** 2003. Unique and conserved features of genome and proteome of SARS-coronavirus, an early split-off from the coronavirus group 2 lineage. J Mol Biol **331:**991–1004. http://dx.doi.org/10.1016/S0022-2836(03)00865-9.
18. **Enjuanes L, Gorbalenya AE, de Groot RJ, Cowley JA, Ziebuhr J, Snijder EJ.** 2008. The Nidovirales, p 419–430. *In* Mahy BWJ, Van Regenmortel M, Walker P, Majumder-Russell D (ed), Encyclopedia of virology, 3rd ed. Elsevier Ltd., Oxford, United Kingdom.
19. **Torres J, Parthasarathy K, Lin X, Saravanan R, Liu DX.** 2006. Model of a putative pore: the pentameric alpha-helical bundle of SARS coronavirus E protein in lipid bilayers. Biophys J **91:**938–947. http://dx.doi.org/10.1529/biophysj.105.080119.
20. **Verdia-Baguena C, Nieto-Torres JL, Alcaraz A, Dediego ML, Torres J, Aguilella VM, Enjuanes L.** 2012. Coronavirus E protein forms ion channels with functionally and structurally-involved membrane lipids. Virology **432:**485–494. http://dx.doi.org/10.1016/j.virol.2012.07.005.
21. **Verdia-Baguena C, Nieto-Torres JL, Alcaraz A, Dediego ML, Enjuanes L, Aguilella VM.** 2013. Analysis of SARS-CoV E protein ion channel activity by tuning the protein and lipid charge. Biochim Biophys Acta **1828:**2026–2031. http://dx.doi.org/10.1016/j.bbamem.2013.05.008.
22. **Pervushin K, Tan E, Parthasarathy K, Lin X, Jiang FL, Yu D, Vararattanavech A, Soong TW, Liu DX, Torres J.** 2009. Structure and inhibition of the SARS coronavirus envelope protein ion channel. PLoS Pathog **5:**e1000511. http://dx.doi.org/10.1371/journal.ppat.1000511.
23. **Nal B, Chan C, Kien F, Siu L, Tse J, Chu K, Kam J, Staropoli I, Crescenzo-Chaigne B, Escriou N, van der Werf S, Yuen KY, Altmeyer R.** 2005. Differential maturation and subcellular localization of severe

acute respiratory syndrome coronavirus surface proteins S, M and E. J Gen Virol **86:**1423–1434. http://dx.doi.org/10.1099/vir.0.80671-0.
24. **Maeda J, Repass JF, Maeda A, Makino S.** 2001. Membrane topology of coronavirus E protein. Virology **281:**163–169. http://dx.doi.org/10.1006/viro.2001.0818.
25. **Nieto-Torres JL, Dediego ML, Alvarez E, Jimenez-Guardeno JM, Regla-Nava JA, Llorente M, Kremer L, Shuo S, Enjuanes L.** 2011. Subcellular location and topology of severe acute respiratory syndrome coronavirus envelope protein. Virology **415:**69–82. http://dx.doi.org/10.1016/j.virol.2011.03.029.
26. **Ye Y, Hogue BG.** 2007. Role of the coronavirus E viroporin protein transmembrane domain in virus assembly. J Virol **81:**3597–3607. http://dx.doi.org/10.1128/JVI.01472-06.
27. **Ruch TR, Machamer CE.** 2012. The coronavirus E protein: assembly and beyond. Viruses **4:**363–382. http://dx.doi.org/10.3390/v4030363.
28. **DeDiego ML, Alvarez E, Almazan F, Rejas MT, Lamirande E, Roberts A, Shieh WJ, Zaki SR, Subbarao K, Enjuanes L.** 2007. A severe acute respiratory syndrome coronavirus that lacks the E gene is attenuated *in vitro* and *in vivo*. J Virol **81:**1701–1713. http://dx.doi.org/10.1128/JVI.01467-06.
29. **DeDiego ML, Pewe L, Alvarez E, Rejas MT, Perlman S, Enjuanes L.** 2008. Pathogenicity of severe acute respiratory coronavirus deletion mutants in hACE-2 transgenic mice. Virology **376:**379–389. http://dx.doi.org/10.1016/j.virol.2008.03.005.
30. **Lamirande EW, DeDiego ML, Roberts A, Jackson JP, Alvarez E, Sheahan T, Shieh WJ, Zaki SR, Baric R, Enjuanes L, Subbarao K.** 2008. A live attenuated SARS coronavirus is immunogenic and efficacious in golden Syrian hamsters. J Virol **82:**7721–7724. http://dx.doi.org/10.1128/JVI.00304-08.
31. **Netland J, DeDiego ML, Zhao J, Fett C, Alvarez E, Nieto-Torres JL, Enjuanes L, Perlman S.** 2010. Immunization with an attenuated severe acute respiratory syndrome coronavirus deleted in E protein protects against lethal respiratory disease. Virology **399:**120–128. http://dx.doi.org/10.1016/j.virol.2010.01.004.
32. **Fett C, DeDiego ML, Regla-Nava JA, Enjuanes L, Perlman S.** 2013. Complete protection against severe acute respiratory syndrome coronavirus-mediated lethal respiratory disease in aged mice by immunization with a mouse-adapted virus lacking E protein. J Virol **87:**6551–6559. http://dx.doi.org/10.1128/JVI.00087-13.
33. **DeDiego ML, Nieto-Torres JL, Jimenez-Guardeno JM, Regla-Nava JA, Alvarez E, Oliveros JC, Zhao J, Fett C, Perlman S, Enjuanes L.** 2011. Severe acute respiratory syndrome coronavirus envelope protein regulates cell stress response and apoptosis. PLoS Pathog **7:**e1002315. http://dx.doi.org/10.1371/journal.ppat.1002315.
34. **Ware LB, Matthay MA.** 2000. The acute respiratory distress syndrome. N Engl J Med **342:**1334–1349. http://dx.doi.org/10.1056/NEJM200005043421806.
35. **Gralinski LE, Bankhead A, III, Jeng S, Menachery VD, Proll S, Belisle SE, Matzke M, Webb-Robertson BJ, Luna ML, Shukla AK, Ferris MT, Bolles M, Chang J, Aicher L, Waters KM, Smith RD, Metz TO, Law GL, Katze MG, McWeeney S, Baric RS.** 2013. Mechanisms of severe acute respiratory syndrome coronavirus-induced acute lung injury. mBio **4**(4): e00271–13. http://dx.doi.org/10.1128/mBio.00271-13.
36. **Franks TJ, Chong PY, Chui P, Galvin JR, Lourens RM, Reid AH, Selbs E, McEvoy CP, Hayden CD, Fukuoka J, Taubenberger JK, Travis WD.** 2003. Lung pathology of severe acute respiratory syndrome (SARS): a study of 8 autopsy cases from Singapore. Hum Pathol **34:**743–748. http://dx.doi.org/10.1016/S0046-8177(03)00367-8.
37. **Nieto-Torres JL, Dediego ML, Verdia-Baguena C, Jimenez-Guardeno JM, Regla-Nava JA, Fernandez-Delgado R, Castano-Rodriguez C, Alcaraz A, Torres J, Aguilella VM, Enjuanes L.** 2014. Severe acute respiratory syndrome coronavirus envelope protein ion channel activity promotes virus fitness and pathogenesis. PLoS Pathog **10:**e1004077. http://dx.doi.org/10.1371/journal.ppat.1004077.
38. **Lee N, Hui D, Wu A, Chan P, Cameron P, Joynt G, Ahuja A, Yung MY, Leung CB, To KF, Lui SF, Szeto CC, Chung S, Sung JJY.** 2003. A major outbreak of severe acute respiratory syndrome in Hong Kong. N Engl J Med **348:**1986–1994. http://dx.doi.org/10.1056/NEJMoa030685.
39. **Yen YT, Liao F, Hsiao CH, Kao CL, Chen YC, Wu-Hsieh BA.** 2006. Modeling the early events of severe acute respiratory syndrome coronavirus infection *in vitro*. J Virol **80:**2684–2693. http://dx.doi.org/10.1128/JVI.80.6.2684-2693.2006.
40. **Chien JY, Hsueh PR, Cheng WC, Yu CJ, Yang PC.** 2006. Temporal changes in cytokine/chemokine profiles and pulmonary involvement in severe acute respiratory syndrome. Respirology **11:**715–722. http://dx.doi.org/10.1111/j.1440-1843.2006.00942.x.
41. **Wong CK, Lam CW, Wu AK, Ip WK, Lee NL, Chan IH, Lit LC, Hui DS, Chan MH, Chung SS, Sung JJ.** 2004. Plasma inflammatory cytokines and chemokines in severe acute respiratory syndrome. Clin Exp Immunol **136:**95–103. http://dx.doi.org/10.1111/j.1365-2249.2004.02415.x.
42. **Tang NL, Chan PK, Wong CK, To KF, Wu AK, Sung YM, Hui DS, Sung JJ, Lam CW.** 2005. Early enhanced expression of interferon-inducible protein-10 (CXCL-10) and other chemokines predicts adverse outcome in severe acute respiratory syndrome. Clin Chem **51:**2333–2340. http://dx.doi.org/10.1373/clinchem.2005.054460.
43. **Jiang Y, Xu J, Zhou C, Wu Z, Zhong S, Liu J, Luo W, Chen T, Qin Q, Deng P.** 2005. Characterization of cytokine/chemokine profiles of severe acute respiratory syndrome. Am J Respir Crit Care Med **171:**850–857. http://dx.doi.org/10.1164/rccm.200407-857OC.
44. **Cameron MJ, Ran L, Xu L, Danesh A, Bermejo-Martin JF, Cameron CM, Muller MP, Gold WL, Richardson SE, Poutanen SM, Willey BM, DeVries ME, Fang Y, Seneviratne C, Bosinger SE, Persad D, Wilkinson P, Greller LD, Somogyi R, Humar A, Keshavjee S, Louie M, Loeb MB, Brunton J, McGeer AJ, Kelvin DJ.** 2007. Interferon-mediated immunopathological events are associated with atypical innate and adaptive immune responses in patients with severe acute respiratory syndrome. J Virol **81:**8692–8706. http://dx.doi.org/10.1128/JVI.00527-07.
45. **Lam CW, Chan MH, Wong CK.** 2004. Severe acute respiratory syndrome: clinical and laboratory manifestations. Clin Biochem Rev **25:**121–132.
46. **de Lang A, Baas T, Teal T, Leijten LM, Rain B, Osterhaus AD, Haagmans BL, Katze MG.** 2007. Functional genomics highlights differential induction of antiviral pathways in the lungs of SARS-CoV-infected macaques. PLoS Pathog **3:**e112. http://dx.doi.org/10.1371/journal.ppat.0030112.
47. **Smits SL, de Lang A, van den Brand JM, Leijten LM, van IWF, Eijkemans MJ, van Amerongen G, Kuiken T, Andeweg AC, Osterhaus AD, Haagmans BL.** 2010. Exacerbated innate host response to SARS-CoV in aged non-human primates. PLoS Pathog **6:**e1000756. http://dx.doi.org/10.1371/journal.ppat.1000756.
48. **Smits SL, van den Brand JM, de Lang A, Leijten LM, van Ijcken WF, van Amerongen G, Osterhaus AD, Andeweg AC, Haagmans BL.** 2011. Distinct severe acute respiratory syndrome coronavirus-induced acute lung injury pathways in two different nonhuman primate species. J Virol **85:**4234–4245. http://dx.doi.org/10.1128/JVI.02395-10.
49. **Baas T, Roberts A, Teal TH, Vogel L, Chen J, Tumpey TM, Katze MG, Subbarao K.** 2008. Genomic analysis reveals age-dependent innate immune responses to severe acute respiratory syndrome coronavirus. J Virol **82:**9465–9476. http://dx.doi.org/10.1128/JVI.00489-08.
50. **Zhao J, Perlman S.** 2010. T cell responses are required for protection from clinical disease and for virus clearance in severe acute respiratory syndrome coronavirus-infected mice. J Virol **84:**9318–9325. http://dx.doi.org/10.1128/JVI.01049-10.
51. **Zhao J, Van Rooijen N, Perlman S.** 2009. Evasion by stealth: inefficient immune activation underlies poor T cell response and severe disease in SARS-CoV-infected mice. PLoS Pathog **5:**e1000636. http://dx.doi.org/10.1371/journal.ppat.1000636.
52. **Chen J, Lau YF, Lamirande EW, Paddock CD, Bartlett JH, Zaki SR, Subbarao K.** 2010. Cellular immune responses to severe acute respiratory syndrome coronavirus (SARS-CoV) infection in senescent BALB/c mice: CD4+ T cells are important in control of SARS-CoV infection. J Virol **84:**1289–1301. http://dx.doi.org/10.1128/JVI.01281-09.
53. **Booth CM, Matukas LM, Tomlinson GA, Rachlis AR, Rose DB, Dwosh HA, Walmsley SL, Mazzulli T, Avendano M, Derkach P, Ephtimios IE, Kitai I, Mederski BD, Shadowitz SB, Gold WL, Hawryluck LA, Rea E, Chenkin JS, Cescon DW, Poutanen SM, Detsky AS.** 2003. Clinical features and short-term outcomes of 144 patients with SARS in the greater Toronto area. JAMA **289:**2801–2809. http://dx.doi.org/10.1001/jama.289.21.JOC30885.
54. **Wong RS, Wu A, To KF, Lee N, Lam CW, Wong CK, Chan PK, Ng MH, Yu LM, Hui DS, Tam JS, Cheng G, Sung JJ.** 2003. Haematological manifestations in patients with severe acute respiratory syndrome: retrospective analysis. BMJ **326:**1358–1362. http://dx.doi.org/10.1136/bmj.326.7403.1358.
55. **Chen J, Subbarao K.** 2007. The immunobiology of SARS*. Annu Rev Immunol **25:**443–472. http://dx.doi.org/10.1146/annurev.immunol.25.022106.141706.

56. **He Z, Zhao C, Dong Q, Zhuang H, Song S, Peng G, Dwyer DE.** 2005. Effects of severe acute respiratory syndrome (SARS) coronavirus infection on peripheral blood lymphocytes and their subsets. Int J Infect Dis **9:**323–330. http://dx.doi.org/10.1016/j.ijid.2004.07.014.
57. **Roberts A, Deming D, Paddock CD, Cheng A, Yount B, Vogel L, Herman BD, Sheahan T, Heise M, Genrich GL, Zaki SR, Baric R, Subbarao K.** 2007. A mouse-adapted SARS-coronavirus causes disease and mortality in BALB/c mice. PLoS Pathog **3:**23–37. http://dx.doi.org/10.1371/journal.ppat.0030005.
58. **DeDiego ML, Nieto-Torres JL, Regla-Nava JA, Jimenez-Guardeno JM, Fernandez-Delgado R, Fett C, Castano-Rodriguez C, Perlman S, Enjuanes L.** 2014. Inhibition of NF-kappaB mediated inflammation in severe acute respiratory syndrome coronavirus-infected mice increases survival. J Virol **88:**913–924. http://dx.doi.org/10.1128/JVI.02576-13.
59. **Almazan F, DeDiego ML, Galan C, Escors D, Alvarez E, Ortego J, Sola I, Zuñiga S, Alonso S, Moreno JL, Nogales A, Capiscol C, Enjuanes L.** 2006. Construction of a SARS-CoV infectious cDNA clone and a replicon to study coronavirus RNA synthesis. J Virol **80:**10900–10906. http://dx.doi.org/10.1128/JVI.00385-06.
60. **Alvarez E, DeDiego ML, Nieto-Torres JL, Jimenez-Guardeno JM, Marcos-Villar L, Enjuanes L.** 2010. The envelope protein of severe acute respiratory syndrome coronavirus interacts with the non-structural protein 3 and is ubiquitinated. Virology **402:**281–291. http://dx.doi.org/10.1016/j.virol.2010.03.015.
61. **Livak KJ, Schmittgen TD.** 2001. Analysis of relative gene expression data using real-time quantitative PCR and the 2(-Delta Delta C(T)) method. Methods **25:**402–408. http://dx.doi.org/10.1006/meth.2001.1262.
62. **Agilent Technologies.** 2008. One-color microarray-based gene expression analysis. Agilent Technologies, Santa Clara, CA.
63. **Smyth GK.** 2004. Linear models and empirical Bayes methods for assessing differential expression in microarray experiments. Stat Appl Genet Mol Biol **3:**Article3. http://dx.doi.org/10.2202/1544-6115.1027.
64. **Benjamini Y, Hochberg Y.** 1995. Controlling the false discovery rate: a practical and powerful approach to multiple testing. J Roy Stat Soc B **57:**289–300.
65. **Ruch TR, Machamer CE.** 2012. A single polar residue and distinct membrane topologies impact the function of the infectious bronchitis coronavirus E protein. PLoS Pathog **8:**e1002674. http://dx.doi.org/10.1371/journal.ppat.1002674.
66. **Siu YL, Teoh KT, Lo J, Chan CM, Kien F, Escriou N, Tsao SW, Nicholls JM, Altmeyer R, Peiris JS, Bruzzone R, Nal B.** 2008. The M, E and N structural proteins of the SARS coronavirus are required for efficient assembly, trafficking and release of virus-like particles. J Virol **82:**11318–11330. http://dx.doi.org/10.1128/JVI.01052-08.
67. **Vennema H, Godeke GJ, Rossen JWA, Voorhout WF, Horzinek MC, Opstelten DJ, Rottier PJM.** 1996. Nucleocapsid-independent assembly of coronavirus-like particles by co-expression of viral envelope protein genes. EMBO J **15:**2020–2028.
68. **Ho Y, Lin PH, Liu CY, Lee SP, Chao YC.** 2004. Assembly of human severe acute respiratory syndrome coronavirus-like particles. Biochem Biophys Res Commun **318:**833–838. http://dx.doi.org/10.1016/j.bbrc.2004.04.111.
69. **Channappanavar R, Zhao J, Perlman S.** 2014. T cell-mediated immune response to respiratory coronaviruses. Immunol Res **59:**118–128. http://dx.doi.org/10.1007/s12026-014-8534-z.
70. **Huang da W, Sherman BT, Lempicki RA.** 2009. Systematic and integrative analysis of large gene lists using DAVID bioinformatics resources. Nat Protoc **4:**44–57. http://dx.doi.org/10.1038/nprot.2008.211.
71. **Kim SJ, Park K, Koeller D, Kim KY, Wakefield LM, Sporn MB, Roberts AB.** 1992. Post-transcriptional regulation of the human transforming growth factor-beta 1 gene. J Biol Chem **267:**13702–13707.
72. **Martin J, Jenkins RH, Bennagi R, Krupa A, Phillips AO, Bowen T, Fraser DJ.** 2011. Post-transcriptional regulation of transforming growth factor beta-1 by microRNA-744. PLoS One **6:**e25044. http://dx.doi.org/10.1371/journal.pone.0025044.
73. **Jimenez-Guardeno JM, Nieto-Torres JL, DeDiego ML, Regla-Nava JA, Fernandez-Delgado R, Castano-Rodriguez C, Enjuanes L.** 2014. The PDZ-binding motif of severe acute respiratory syndrome coronavirus envelope protein is a determinant of viral pathogenesis. PLoS Pathog **10:**e1004320. http://dx.doi.org/10.1371/journal.ppat.1004320.
74. **Teoh KT, Siu YL, Chan WL, Schluter MA, Liu CJ, Peiris JS, Bruzzone R, Margolis B, Nal B.** 2010. The SARS coronavirus E protein interacts with PALS1 and alters tight junction formation and epithelial morphogenesis. Mol Biol Cell **21:**3838–3852. http://dx.doi.org/10.1091/mbc.E10-04-0338.
75. **Cohen JR, Lin LD, Machamer CE.** 2011. Identification of a Golgi complex-targeting signal in the cytoplasmic tail of the severe acute respiratory syndrome coronavirus envelope protein. J Virol **85:**5794–5803. http://dx.doi.org/10.1128/JVI.00060-11.
76. **Puneet P, Moochhala S, Bhatia M.** 2005. Chemokines in acute respiratory distress syndrome. Am J Physiol Lung Cell Mol Physiol **288:**L3–L15. http://dx.doi.org/10.1152/ajplung.00405.2003.
77. **Nagata N, Iwata N, Hasegawa H, Fukushi S, Harashima A, Sato Y, Saijo M, Taguchi F, Morikawa S, Sata T.** 2008. Mouse-passaged severe acute respiratory syndrome-associated coronavirus leads to lethal pulmonary edema and diffuse alveolar damage in adult but not young mice. Am J Pathol **172:**1625–1637. http://dx.doi.org/10.2353/ajpath.2008.071060.
78. **Grommes J, Soehnlein O.** 2011. Contribution of neutrophils to acute lung injury. Mol Med **17:**293–307. http://dx.doi.org/10.2119/molmed.2010.00138.
79. **Tsui PT, Kwok ML, Yuen H, Lai ST.** 2003. Severe acute respiratory syndrome: clinical outcome and prognostic correlates. Emerg Infect Dis **9:**1064–1069. http://dx.doi.org/10.3201/eid0909.030362.
80. **Narasaraju T, Yang E, Samy RP, Ng HH, Poh WP, Liew AA, Phoon MC, van Rooijen N, Chow VT.** 2011. Excessive neutrophils and neutrophil extracellular traps contribute to acute lung injury of influenza pneumonitis. Am J Pathol **179:**199–210. http://dx.doi.org/10.1016/j.ajpath.2011.03.013.
81. **Brandes M, Klauschen F, Kuchen S, Germain RN.** 2013. A systems analysis identifies a feedforward inflammatory circuit leading to lethal influenza infection. Cell **154:**197–212. http://dx.doi.org/10.1016/j.cell.2013.06.013.
82. **Bataki EL, Evans GS, Everard ML.** 2005. Respiratory syncytial virus and neutrophil activation. Clin Exp Immunol **140:**470–477. http://dx.doi.org/10.1111/j.1365-2249.2005.02780.x.
83. **Yasui K, Baba A, Iwasaki Y, Kubo T, Aoyama K, Mori T, Yamazaki T, Kobayashi N, Ishiguro A.** 2005. Neutrophil-mediated inflammation in respiratory syncytial viral bronchiolitis. Pediatr Int **47:**190–195. http://dx.doi.org/10.1111/j.1442-200x.2005.02039.x.
84. **De Filippo K, Dudeck A, Hasenberg M, Nye E, van Rooijen N, Hartmann K, Gunzer M, Roers A, Hogg N.** 2013. Mast cell and macrophage chemokines CXCL1/CXCL2 control the early stage of neutrophil recruitment during tissue inflammation. Blood **121:**4930–4937. http://dx.doi.org/10.1182/blood-2013-02-486217.
85. **Wareing MD, Lyon A, Inglis C, Giannoni F, Charo I, Sarawar SR.** 2007. Chemokine regulation of the inflammatory response to a low-dose influenza infection in CCR2−/− mice. J Leukoc Biol **81:**793–801. http://dx.doi.org/10.1189/jlb.0506299.
86. **Fujiwara N, Kobayashi K.** 2005. Macrophages in inflammation. Curr Drug Targets Inflamm Allergy **4:**281–286. http://dx.doi.org/10.2174/1568010054022024.
87. **Jenkins SJ, Ruckerl D, Cook PC, Jones LH, Finkelman FD, van Rooijen N, MacDonald AS, Allen JE.** 2011. Local macrophage proliferation, rather than recruitment from the blood, is a signature of TH2 inflammation. Science **332:**1284–1288. http://dx.doi.org/10.1126/science.1204351.
88. **Enjuanes L, DeDiego ML, Alvarez E, Deming D, Sheahan T, Baric R.** 2008. Vaccines to prevent severe acute respiratory syndrome coronavirus-induced disease. Virus Res **133:**45–62. http://dx.doi.org/10.1016/j.virusres.2007.01.021.
89. **Graham RL, Donaldson EF, Baric RS.** 2013. A decade after SARS: strategies for controlling emerging coronaviruses. Nat Rev Microbiol **11:**836–848. http://dx.doi.org/10.1038/nrmicro3143.